Annu. Rev. Earth Planet. Sci. 2005. 33:493–530
doi: 10.1146/annurev.earth.32.101802.120325

First published online as a Review in Advance on January 28, 2005

THE INTERIORS OF GIANT PLANETS: Models and Outstanding Questions

Tristan Guillot
Observatoire de la Côte d'Azur, Laboratoire Cassiopée, CNRS UMR 6202, 06304 Nice Cedex 04, France; email: guillot@obs-nice.fr

Key Words extrasolar planets, planet formation, equations of state, planet composition, gravitational moments, tidal heating

■ **Abstract** We know that giant planets played a crucial role in the making of our Solar System. The discovery of giant planets orbiting other stars is a formidable opportunity to learn more about these objects, what their composition is, how various processes influence their structure and evolution, and most importantly how they form. Jupiter, Saturn, Uranus, and Neptune can be studied in detail, mostly from close spacecraft flybys. We can infer that they are all enriched in heavy elements compared to the Sun, with the relative global enrichments increasing with distance to the Sun. We can also infer that they possess dense cores of varied masses. The intercomparison of presently characterized extrasolar giant planets shows that they are also mainly made of hydrogen and helium, but that they either have significantly different amounts of heavy elements, have had different orbital evolutions, or both. Hence, many questions remain and need to be answered to make significant progress on the origins of planets.

Pourquoi l'azur muet et l'espace insondable?
Pourquoi les astres d'or fourmillant comme un sable?
Arthur Rimbaud—Soleil et chair

1. INTRODUCTION

Looking at a starry sky, it is quite vertiginous to think that we are at one of these special epochs in history: Recently, we only knew of the planets in our Solar System. Now, more than 150 giant planets are known to orbit solar-like stars. Our giant planets, Jupiter, Saturn, Uranus, and Neptune, are no longer the only ones that we can characterize. We now know of six extrasolar giant planets transiting in front of their stars for which we can measure with a fair accuracy their mass and radius. We lie on the verge of a true revolution: With ground-based and future space-based transit search programs, we should soon be able to detect and characterize many tens, probably hundreds, of planets orbiting their stars, with the hope of inferring their composition and hence the mechanisms responsible for the formation of planets.

It is a daunting task, too, because we expect that, like for the planets in our Solar System, a rich variety of giant planets will be found with different compositions, different histories, and a number of new or unexpected physical mecanisms at work. We have to classify observations, test theories, and be aware that although simplicity is appealing, it is not always what Nature has in store for us.

This review provides a synthetic approach to the problems posed by "old" and "new" giant planets in the Solar System and outside. It updates a previous review by Stevenson (1982) and expands on the review by Hubbard et al. (2002) by focusing on the mass-radius relations and compositions of giant planets. In Section 2, we see how to construct interior and evolution models of giant planets. Section 3 is devoted to our giant planets, what we can infer from observations, and the questions that remain. I then turn to the new field of extrasolar giant planets, focusing on the close-in, transiting Pegasi planets (also called hot Jupiters). The last section is an attempt to summarize some of the known facts concerning giant planets and provide a few expected milestones for future studies.

2. THE CALCULATION OF INTERIOR MODELS

2.1. A Simple Model

To tell our story, I will use a simple model based on the following assumptions:

1. Giant planets are made of a fluid envelope and possibly a dense central core of $\sim$15 $M_\oplus$ (Earth masses).
2. The envelope is mostly made of hydrogen and helium and trace species (heavy elements); the core is made of an unknown combination of refractory material ("rocks") and more volatile species ("ices," including molecular species such as H_2O water, CH_4 methane, and NH_3 ammonia in the fluid state).
3. Contrary to solid planets, viscosity is negligible throughout giant planets.
4. In most cases, rotation and magnetic fields can be neglected.
5. Giant planets were formed from an extended, high-entropy, high-luminosity state.

These assumptions can only be justified a posteriori: They are the result of our knowledge of observed giant planets and of inferences about the mechanisms that led to their formation. I describe below how this simple model predicts the global properties of giant planets between 1/20 to 20 M_J (approximately 15 and 6000 $M_\oplus$) and how they compare with observations.

2.2. Basic Equations

As a consequence of our assumptions, the structure and evolution of a giant planet is governed by the following hydrostatic, thermodynamic, mass conservation, and

energy conservation equations:

$$\frac{\partial P}{\partial r} = -\rho g, \tag{1}$$

$$\frac{\partial T}{\partial r} = \frac{\partial P}{\partial r}\frac{T}{P}\nabla_T, \tag{2}$$

$$\frac{\partial m}{\partial r} = 4\pi r^2 \rho, \tag{3}$$

$$\frac{\partial L}{\partial r} = 4\pi r^2 \rho \left(\dot{\epsilon} - T\frac{\partial S}{\partial t}\right), \tag{4}$$

where P is the pressure, ρ is the density, and $g = Gm/r^2$ is the gravity (m is the mass, r the radius, and G is the gravitational constant). The temperature gradient $\nabla_T \equiv (d \ln T/d \ln P)$ depends on the process by which the internal heat is transported. L is the intrinsic luminosity; t is the time; S is the specific entropy (per unit mass); and $\dot{\epsilon}$ accounts for the sources of energy owing to, e.g., radioactivity or nuclear reactions. Generally, it is a good approximation to assume $\dot{\epsilon} \sim 0$ for objects less massive than $\sim$13 M_J, i.e., too cold to even burn deuterium (but in certain conditions this term may be useful, even for low-mass planets).

The boundary condition at the center is trivial: $r = 0 (m = 0, L = 0)$. The external boundary condition is more difficult to obtain because it depends on how energy is transported in the atmosphere. One possibility is to use the Eddington approximation and to write (e.g. Chandrasekhar 1939) $r = R$ ($T_0 = T_{\rm eff}$, $P_0 = 2/3\, g/\kappa$), where $T_{\rm eff}$ is the effective temperature and κ is the opacity in $\mathrm{cm^2\,g^{-1}}$. Note, for example, that in the case of Jupiter $T_{\rm eff} = 124$ K, $g = 2600\,\mathrm{cm\,s^{-2}}$, and $\kappa \approx 5 \times 10^{-2} (P/1\,\mathrm{bar})\,\mathrm{cm^2\,g^{-1}}$. This implies $P_0 \approx 0.2$ bar, which is actually close to Jupiter's tropopause, where $T \approx 110$ K.

Generally, one has to use an atmospheric model relating the temperature and pressure at a given level to the radius R, intrinsic luminosity L, and incoming stellar luminosity $L_{*\rm p}$: $r = R$ [$T_0 = T_0(R, L, L_{*\rm p})$, $P_0 = P_0(R, L, L_{*\rm p})$]. P_0 is chosen to satisfy the condition that the corresponding optical depth at that level should be much larger than unity. If the stellar flux is absorbed mostly in a convective zone then the problem can be simplified by using $T_0(R, L, L_{*\rm p}) \approx T_0(R, L + L_{*\rm p}, 0)$ (e.g., Hubbard 1977). An example of such a model is described by Saumon et al. (1996) and Hubbard et al. (2002) and is used hereafter to model the planets in the low irradiation limit.

2.3. High-Pressure Physics and Equations of State

In terms of pressures and temperatures, the interiors of giant planets lie in a region for which accurate equations of state (EOS) are extremely difficult to calculate. This is because molecules, atoms, and ions can coexist in a fluid that is partially degenerate (free electrons have energies that are determined both by quantic and thermal effects) and partially coupled (coulombian interactions between ions are

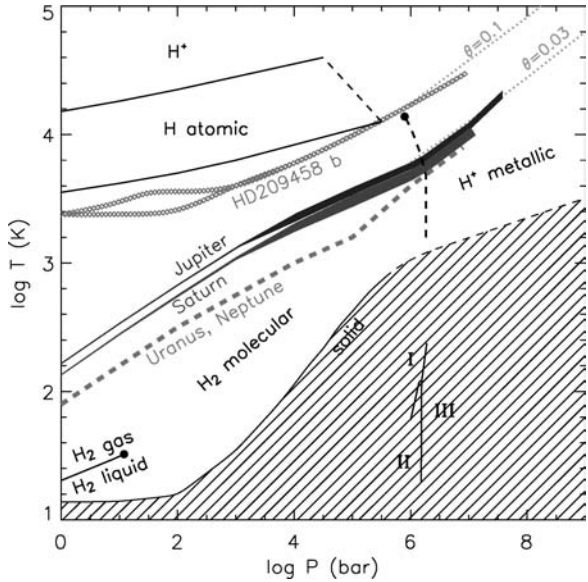

Figure 1 Phase diagram for hydrogen with the main phase transitions occurring in the fluid or gas phase. The temperature-pressure profiles for Jupiter, Saturn, Uranus, Neptune, and HD209458b are shown. The dashed, nearly vertical line near 1 Mbar is indicative of the molecular to metallic transition (here it represents the so-called plasma phase transition as calculated by Saumon et al. 2000). The region in which hydrogen is in solid phase (Datchi et al. 2000, Gregoryanz et al. 2003) is represented as a dashed area. The three phases (I, II, III) of solid hydrogen are shown (see Mao & Hemley 1994). Values of the degeneracy parameter θ are indicated as dotted lines to the upper right corner of the figure.

not dominant but must be taken into account). The presence of many elements and their possible interactions further complicate matters. For lack of space, this section mainly focuses on hydrogen whose EOS has seen the most important developments in recent years. A phase diagram of hydrogen (Figure 1) illustrates some of the important phenomena that occur in giant planets.

The photospheres of giant planets are generally relatively cold (50 to 3000 K) and at low pressure (0.1 to 10 bar, or 10^4 to 10^6 Pa) so that hydrogen is in molecular form and the perfect gas conditions apply. As one goes deeper into the interior, hydrogen and helium progressively become fluid. [The perfect gas relation tends to underestimate the pressure by 10% or more when the density becomes larger than approximately $0.02\,\mathrm{g\,cm^{-3}}$ ($P \gtrsim 1$ kbar in the case of Jupiter).]

Characteristic interior pressures are considerably larger, however; as implied by Equations 1 and 3, $P_c \approx GM^2/R^4$, of the order of 10–100 Mbar for Jupiter and Saturn. At these pressures and the corresponding densities, the Fermi temperature

T_F is larger than 10^5 K. This implies that electrons are degenerate. Figure 1 shows that inside Jupiter, Saturn, and HD209458b, but also for giant planets in general for most of their history, the degeneracy parameter $\theta = T/T_F$ is between 0.1 and 0.03. Therefore, the energy of electrons in the interior is expected to be only slightly larger than their nonrelativistic, fully degenerate limit: $u_e \geq 3/5\, kT_F = 15.6\,(\rho/\mu_e)^{2/3}$ eV, where k is Boltzmann's constant, μ_e is the number of electrons per Nucleon, and ρ is the density in g cm^{-3}. For pure hydrogen, when the density reaches $\sim$0.8 g cm^{-3}, the average energy of electrons becomes larger than hydrogen's ionization potential, even at zero temperature: Hydrogen pressure-ionizes and becomes metallic. This molecular to metallic transition occurs near Mbar pressures, but exactly how this happens remains unclear because of the complex interplay of thermal, coulombian, and degeneracy effects (in particular, whether hydrogen metallizes into an atomic state H^+—as suggested in Figure 1—or first metallizes in the molecular state H_2 remains to be clarified).

Recent laboratory measurements on fluid deuterium have been able to reach pressures above $\gtrsim$1 Mbar and provide new data in a region where the EOS remains most uncertain. Gas-guns experiments have been able to measure the reshock temperature (Holmes et al. 1995), near $T \sim 5000$ K, $P \sim 0.8$ Mbar, and a rise in the conductivity of molecular hydrogen up to $T \sim 3000$ K, $P \sim 1.4$ Mbar, a sign that metallicity may have been reached (Weir et al. 1996). The following few years have seen the development of laser-induced shock compression (Da Silva et al. 1997, Collins et al. 1998), pulsed-power shock compression (Knudson et al. 2002, 2004), and convergent shock wave experiments (Belov et al. 2002, Boriskov et al. 2003) in a high-pressure ($P = 0.3 - 4$ Mbar), high-temperature ($T \sim 6000 - 10^5$ K) regime. Unfortunately, experimental results along the principal Hugoniot of deuterium do not agree in this pressure range. Laser compression data give a maximum compression of $\sim$6, whereas the pulsed-power compression experiments and the convergent shock wave experiments find a value of $\sim$4. Models that are partly calibrated with experimental data (Saumon et al. 1995, 2000; Ross 1998; Ross & Yang 2001) obtain a generally good agreement with the laser-compression data. However, the fact that independant experiments based on first principles yield low compressions (e.g., Militzer & Ceperley 2001, Desjarlais 2003, Boney et al. 2004) strongly favors this solution.

The question of the existence of a first-order molecular to metallic transition of hydrogen (i.e., molecular dissociation and ionization occur simultaneously and discontinuously at the so-called plasma phase transition, or PPT) remains, however. The critical line shown in Figure 1 corresponds to calculations by Saumon et al. (2000), but may be caused by artefacts in the free energy calculation. Recent density functional theory (DFT) simulations by Bonev et al. (2004) indicate the possibility of a first-order liquid-liquid transition, but other path-integral calculations (Militzer & Ceperley 2001) do not. It is crucial to assess the existence of such a PPT because it would affect both convection and chemical composition in the giant planets.

A clear result from Figure 1 is that, as first shown by Hubbard (1968), the interiors of the hydrogen-helium giant planets are fluid, whatever their age (an isolated

Jupiter should begin partial solidification only after at least $\sim 10^3$ Ga of evolution). For Uranus and Neptune, the situation is actually more complex because at large pressures they are not expected to contain hydrogen, but numerical simulations show that ices in their interior should be fluid as well (Cavazzoni et al. 1999).

Models of the interiors of giant planets require thermodynamically consistent EOSs calculated over the entire domain of pressure and temperature spanned by the planets during their evolution. Elements other than hydrogen, most importantly helium, should be consistently included. Such a calculation is a daunting task, and the only recent attempt at such an astrophysical EOS for substellar objects is that by Saumon et al. (1995). Another set of EOSs reproducing either the high- or low-compression results was calculated by Saumon & Guillot (2004) specifically for the calculation of present-day models of Jupiter and Saturn.

These EOSs have so far included other elements (including helium), only in a very approximate way, i.e., with EOSs for helium and heavy elements that are based on interpolations between somewhat ideal regimes, using an additive volume law, and neglecting the possibility of existence of phase separations (see Hubbard et al. 2002 and Guillot et al. 2004 for further discussions).

2.4. Heat Transport

Giant planets possess hot interiors, implying that a relatively large amount of energy has to be transported from the deep regions of the planets to their surface. This can either be done by radiation, conduction, or, if these processes are not sufficient, by convection. Convection is generally ensured by the rapid rise of the opacity with increasing pressure and temperature. At pressures of one bar or more and relatively low temperatures (less than 1000 K), the three dominant sources of opacities are water, methane, and collision-induced absorption by hydrogen molecules.

However, in the intermediate temperature range between $\sim$1200 and 1500 K, the Rosseland opacity owing to the hydrogen and helium absorption behaves differently: The absorption at any given wavelength increases with density, but because the temperature also rises, the photons are emitted at shorter wavelengths where the monochromatic absorption is smaller. As a consequence, the opacity can decrease. This was shown by Guillot et al. (1994) to potentially lead to the presence of a deep radiative zone in the interiors of Jupiter, Saturn, and Uranus.

This problem must be reanalyzed in the light of recent observations of brown dwarfs. Their spectra show unexpectedly wide sodium and potassium absorption lines (see Burrows et al. 2000a) in spectral regions where hydrogen, helium, water, methane, and ammonia are relatively transparent. It thus appears that the added contribution of these elements (if they are indeed present) would wipe out any radiative region at these levels (Guillot et al. 2004).

At temperatures above 1500 $\sim$ 2000 K, two important sources of opacity appear: (*a*) The rising number of electrons greatly enhances the absorption of H_2^- and H^-; and (*b*) TiO, a very strong absorber at visible wavelengths is freed by the

vaporization of $CaTiO_3$. Again, the opacity rises rapidly, which ensures a convective transport of the heat. Still deeper, conduction by free electrons becomes more efficient, but the densities are found not to be high enough for this process to be significant, except perhaps near the central core (see Hubbard 1968, Stevenson & Salpeter 1977).

However, because irradiated giant planets do develop a radiative zone, Rosseland opacity tables covering the proper range of temperatures and pressures are needed. A pure hydrogen-helium mixture table has been calculated by Lenzuni et al. (1991). Opacities for solar composition, including grains, are available from Alexander & Ferguson (1994), but they do not include alkali metals and up-to-date data on water, methane, and TiO absorption. Guillot (1999a) provides a grain-free, alkali-free table that is limited to low-temperature regimes. The calculations hereafter use opacities provided by Allard on the basis of calculations for brown dwarfs of solar composition, including grains and alkali metals (Allard et al. 2001).

2.5. The Contraction and Cooling Histories of Giant Planets

The interiors of giant planets are expected to evolve with time from a high entropy, high θ value, hot initial state to a low entropy, low θ, cold degenerate state. The essential physics behind this evolution can be derived from the well-known virial theorem and the energy conservation equation, which link the planet's internal energy E_i, gravitational energy E_g, and luminosity through

$$\xi E_i + E_g = 0, \tag{5}$$

$$L = -\frac{\xi - 1}{\xi}\frac{dE_g}{dt}, \tag{6}$$

where $\xi = \int_0^M 3(P/\rho)\mathrm{dm}/\int_0^M u dm \approx \langle 3P/\rho u\rangle$ and u is the specific internal energy. For a diatomic perfect gas, $\xi = 3.2$; for fully degenerate nonrelativistic electrons, $\xi = 2$.

Thus, for a giant planet or brown dwarf beginning its life mostly as a perfect H_2 gas, two thirds of the energy gained by contraction is radiated away, one third being used to increase E_i. The internal energy being proportional to the temperature, the effect is to heat up the planet. This represents the slightly counter-intuitive but well-known effect that a star or giant planet initially heats up while radiating a significant luminosity.

Let us now move further in the evolution, when the contraction has proceeded to a point where the electrons have become degenerate. For simplicity, I ignore Coulombian interactions and exchange terms, and I assume that the internal energy can be written as $E_i = E_{el} + E_{ion}$ and that furthermore, $E_{el} \gg E_{ion}$ (θ is small). Because $\xi \approx 2$, we know that half of the gravitational potential energy is radiated away and half of it goes into internal energy. The problem is to decide how this energy is split into an electronic and an ionic part. The gravitational energy changes with some average value of the interior density as $E_g \propto 1/R \propto \rho^{1/3}$. The energy of the degenerate electrons is essentially the Fermi energy: $E_{el} \propto \rho^{2/3}$.

Therefore, $\dot{E}_{\rm el} \approx 2(E_{\rm e}/E_{\rm g})\dot{E}_{\rm g}$. Using the virial theorem, this yields

$$\dot{E}_{\rm e} \approx -\dot{E}_{\rm g} \approx 2L \tag{7}$$

$$L \approx -\dot{E}_{\rm ion} \propto -\dot{T}. \tag{8}$$

The gravitational energy lost is entirely absorbed by the degenerate electrons, and the observed luminosity is due to the thermal cooling of the ions.

Several simplifications limit the applicability of this result (that would be valid in the white dwarf regime). In particular, the Coulombian and exchange terms in the EOS introduce negative contributions that cannot be neglected. However, the approach is useful to grasp how the evolution proceeds: In its very early stages, the planet is very compressible. It follows a standard Kelvin-Helmoltz contraction. When degeneracy sets in, the compressibility becomes much smaller ($\alpha T \sim 0.1$, where α is the coefficient of thermal expansion), and the planet gets its luminosity mostly from the thermal cooling of the ions. The luminosity can be written in terms of a modified Kelvin-Helmoltz formula:

$$L \approx \eta \frac{GM^2}{R\tau}, \tag{9}$$

where τ is the age, and η is a factor that hides most of the complex physics. In the approximation that Coulombian and exchange terms can be neglected, $\eta \approx \theta/(\theta+1)$. The poor compressibility of giant planets in their mature evolution stages imply that $\eta \ll 1$: The luminosity is not obtained from the entire gravitational potential but from the much more limited reservoir constituted by the thermal internal energy. Equation 9 shows that to first order, $\log L \propto -\log \tau$: Very little time is spent at high luminosity values. In other words, the problem is (in most cases) weakly sensitive to initial conditions.

Figure 2 shows calculated luminosities in the framework of our simple model. Compared to Equation 9, calculated luminosities are consistent with $\eta \approx 0.01$ to 0.03. The lower luminosities obtained in the presence of a core and of more heavy elements are due to an earlier contraction and quicker loss of the internal heat. As model *b* would be appropropriate to explain Saturn's radius (see next section), it can be seen that the planet emits more heat than predicted by homogeneous contraction models. The cases of Uranus and Neptune are more complex and cannot be directly compared with the models in Figure 2, which neglect the thermal heat content of the central core.

2.6. Mass-Radius Relation

The relation between mass and radius has very fundamental astrophysical applications. Most importantly, it allows one to infer the gross composition of an object from a measurement of its mass and radius. This is especially relevant in the context of the discovery of extrasolar planets with both radial velocimetry and the transit method, as the two techniques yield relatively accurate determination of M and R.

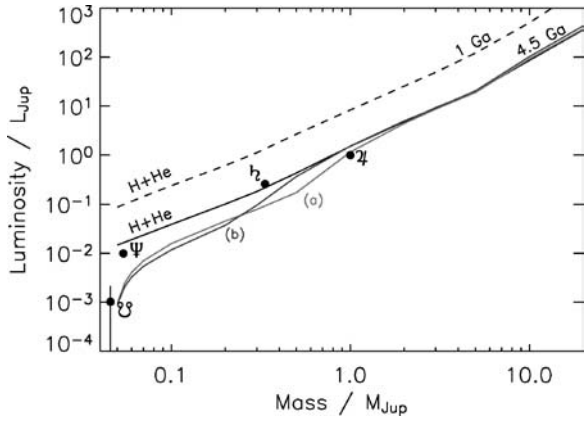

Figure 2 Luminosity versus mass for giant planets after 4.5 Ga of evolution compared to measured values for our four giant planets (including the significant uncertainty on Uranus' luminosity). The lines correspond to H + He: a pure hydrogen-helium composition with a helium mass mixing ratio $Y = 0.25$, *a*: a model with $Y = 0.30$ and a 15 $M_\oplus$ core; and *b*: the same model but with $Y = 0.36$.

Figure 3 shows the mass-radius relation for isolated or nearly isolated gaseous planets based on our simple model and various assumptions on their composition. The curves have a local maximum near 4 M_J: At small masses, the compression is rather small so that the radius increases with mass. At large masses, degeneracy sets in and the radius decreases with mass.

This can be understood on the basis of polytropic models based on the assumption that $P = K\rho^{1+1/n}$, where K and n are constants. Because of degeneracy, a planet of large mass tends to have $n \to 1.5$, whereas a planet of smaller mass will be less compressible ($n \to 0$). Indeed, it can be shown that in the inner 70% to 80% of radius isolated planets of 10, 1, and 0.1 M_J have $n = 1.3$, 1.0 and 0.6, respectively. From polytropic equations (e.g., Chandrasekhar 1939),

$$R \propto K^{\frac{n}{3-n}} M^{\frac{1-n}{3-n}}. \tag{10}$$

Assuming that K is independent of mass, one gets $R \propto M^{-0.18}$, M^0, and $M^{0.16}$ for $M = 10, 1,$ and 0.1 M_J, respectively, which is in relatively good agreement with Figure 3 (the small discrepancies are due to the fact that the intrinsic luminosity and hence K depend on the mass considered).

Figure 3 shows that the planets in our Solar System are not made of pure hydrogen and helium: Their radii lie below that predicted for $Y = 0.25$ objects. Indeed, Jupiter, Saturn, and the two ice-giants Uranus and Neptune contain a growing proportion of heavy elements. The theoretical curves for olivine and ice planets predict even smaller radii, however: Even Uranus and Neptune contain 10% to 20% of their mass as hydrogen and helium.

The extrasolar planets detected so far (see Table 3) all lie above the pure hydrogen-helium curve. This is due to the fact that these planets have their

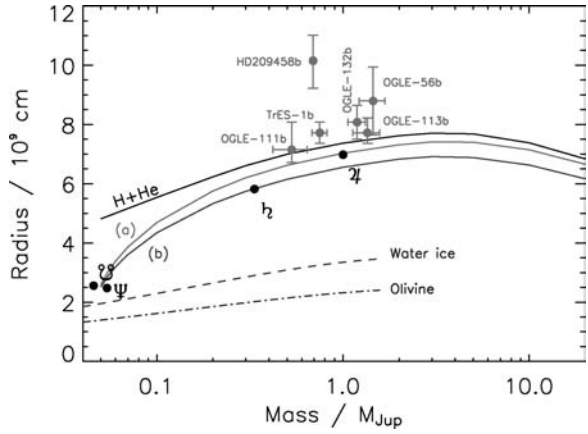

Figure 3 Radius versus mass for giant planets after 4.5 Ga of evolution compared to measured values for our four giant planets and four known extrasolar planets. As in Figure 2, the lines correspond to H + He: a pure hydrogen-helium composition with $Y = 0.25$; *a*: a model with $Y = 0.30$ and a $15\,M_\oplus$ core; and *b*: the same model but with $Y = 0.36$. An approximate mass-radius relation for zero-temperature water and olivine planets is shown as dashed and dash-dotted lines, respectively (courtesy of W.B. Hubbard).

evolutions dominated by the intense stellar irradiation they receive. Thermal effects are no longer negligible: Using the Eddington approximation, assuming $\kappa \propto P$ and a perfect gas relation in the atmosphere, one can show that $K \propto (M/R^2)^{-1/2n}$ and therefore $R \propto M^{\frac{1/2-n}{2-n}}$. With $n = 1$, one finds $R \propto M^{-1/2}$. Strongly irradiated hydrogen-helium planets of small masses are hence expected to have the largest radii, which qualitatively explains the positions of the extrasolar planets in Figure 3. Note that this estimate implicitly assumes that n is constant throughout the planet. The real situation is more complex because of the growth of a deep radiative region in most irradiated planets and because of structural changes between the degenerate interior and the perfect gas atmosphere.

2.7. Rotation and the Figures of Planets

The mass and radius of a planet informs us of its global composition. Because planets are also rotating, one is allowed to obtain more information on their deep interior structure. The hydrostatic equation becomes more complex, however:

$$\frac{\nabla P}{\rho} = \nabla \left(G \iiint \frac{\rho(\mathbf{r}')}{|\mathbf{r} - \mathbf{r}'|} d^3\mathbf{r}' \right) - \boldsymbol{\Omega} \times (\boldsymbol{\Omega} \times \mathbf{r}), \tag{11}$$

where $\boldsymbol{\Omega}$ is the rotation vector. The resolution of Equation 11 is a complex problem. It can, however, be somewhat simplified by assuming that $|\boldsymbol{\Omega}| \equiv \omega$ is such that the centrifugal force can be derived from a potential. The hydrostatic equilibrium

then writes $\nabla P = \rho \nabla U$, and the figure of the rotating planet is then defined by the $U =$ cte level surface.

One can show (e.g., Zharkov & Trubitsyn 1978) that the hydrostatic equation of a fluid planet can then be written in terms of the mean radius $\bar{r}$ (the radius of a sphere containing the same volume as that enclosed by the considered equipotential surface):

$$\frac{1}{\rho}\frac{\partial P}{\partial \bar{r}} = -\frac{Gm}{\bar{r}^2} + \frac{2}{3}\omega^2 \bar{r} + \frac{GM}{\bar{R}^3}\bar{r}\varphi_\omega, \tag{12}$$

where M and $\bar{R}$ are the total mass and mean radius of the planet, and φ_ω is a slowly varying function of $\bar{r}$. (In the case of Jupiter, φ_ω varies from approximately 2×10^{-3} at the center to 4×10^{-3} at the surface.) Equations 2–4 remain the same with the hypothesis that the level surfaces for the pressure, temperature, and luminosity are equipotentials. The significance of rotation is measured by the ratio of the centrifugal acceleration to the gravity:

$$q = \frac{\omega^2 R_{\text{eq}}^3}{GM}. \tag{13}$$

The external gravitational potential of the planet is (assuming hydrostatic equilibrium)

$$V_{\text{ext}}(r, \cos\theta) = \frac{GM}{r}\left[1 - \sum_{n=1}^{\infty}\left(\frac{a}{r}\right)^{2n} J_{2n} P_{2n}(\cos\theta)\right], \tag{14}$$

where the coefficients J_{2n} are the planet's gravitational moments, the P_{2n} are Legendre polynomials, and the θ is the colatitude. The Js can be measured by a spacecraft coming close to the planet, preferably on a polar orbit. Together with the mass, this provides a constraint on the interior density profile (see Zharkov & Trubitsyn 1974):

$$M = \iiint \rho(r, \theta) d^3\tau,$$

$$J_{2i} = -\frac{1}{M R_{\text{eq}}^{2i}} \iiint \rho(r, \theta) r^{2i} P_{2i}(\cos\theta) d^3\tau,$$

where $d\tau$ is a volume element and the integrals are performed over the entire volume of the planet.

Figure 4 shows how the different layers inside a planet contribute to the mass and the gravitational moments. The figure applies to Jupiter, but would remain very similar for other planets. Measured gravitational moments thus provide information on the external levels of a planet. It is only indirectly, through the constraints on the outer envelope, that the presence of a central core can be inferred. As a consequence, it is impossible to determine this core's state (liquid or solid), structure (differentiated, partially mixed with the envelope) and composition (rock, ice, helium, etc.).

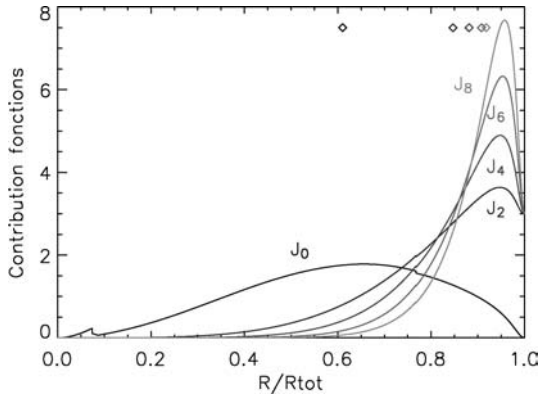

Figure 4 Contribution of the level radii to the gravitational moments of Jupiter. J_0 is equivalent to the planet's mass. The small discontinuities are caused by the following transitions, from left to right: core/envelope, helium rich/helium poor (metallic/molecular). Diamonds indicate the median radius for each moment.

For planets outside the Solar System, although measuring their gravitational potential is utopic, their oblateness may be reachable with future space transit observations (Seager & Hui 2002). Because the oblateness e is, to first order, proportionnal to q,

$$e = \frac{R_{\rm eq}}{R_{\rm eq} - R_{\rm pol}} \approx \left(\frac{3}{2}\Lambda_2 + \frac{1}{2}\right) \tag{15}$$

(where $\Lambda_2 = J_2/q \approx 0.1$ to 0.2), it may be possible to obtain their rotation rate, or with a rotation measured from another method, a first constraint on their interior structure.

3. JUPITER, SATURN, URANUS, AND NEPTUNE

3.1. Main Observational Data

The mass of the giant planets can be obtained with great accuracy from the observation of the motions of their natural satellites: 317.834, 95.161, 14.538, and 17.148 times the mass of Earth ($1\,M_\oplus = 5.97369 \times 10^{27}$g) for Jupiter, Saturn, Uranus, and Neptune, respectively. The more precise determination of their gravity fields listed in Table 1 have been obtained by the *Pioneer* and *Voyager* space missions.

Table 1 also indicates the radii obtained with the greatest accuracy by radio-occultation experiments. By convention, these radii and gravitational moments correspond to the 1 bar pressure level. The rotation periods are measured from the variations of the planets' magnetic fields (system III) and are believed to be tied

TABLE 1 Characteristics of the gravity fields and radii

	Jupiter	**Saturn**	**Uranus**	**Neptune**
$M \times 10^{-29}$ [g]	18.986112(15)[a]	5.684640(30)[b]	0.8683205(34)[c]	1.0243542(31)[d]
$R_{eq} \times 10^{-9}$ [cm]	7.1492(4)[e]	6.0268(4)[f]	2.5559(4)[g]	2.4766(15)[g]
$R_{pol} \times 10^{-9}$ [cm]	6.6854(10)[e]	5.4364(10)[f]	2.4973(20)[g]	2.4342(30)[g]
$\bar{R} \times 10^{-9}$ [cm]	6.9894(6)[h]	5.8210(6)[h]	2.5364(10)[i]	2.4625(20)[i]
$\bar{\rho}$ [g cm^{-3}]	1.3275(4)	0.6880(2)	1.2704(15)	1.6377(40)
$J_2 \times 10^2$	1.4697(1)[a]	1.6332(10)[b]	0.35160(32)[c]	0.3539(10)[d]
$J_4 \times 10^4$	−5.84(5)[a]	−9.19(40)[b]	−0.354(41)[c]	−0.28(22)[d]
$J_6 \times 10^4$	0.31(20)[a]	1.04(50)[b]	...	...
$P_\omega \times 10^{-4}$ [s]	3.57297(41)[j]	3.83577(47)[j]	6.206(4)[k]	5.800(20)[l]
q	0.08923(5)	0.15491(10)	0.02951(5)	0.02609(23)
C/MR_{eq}^2	0.258	0.220	0.230	0.241

The numbers in parentheses are the uncertainty in the last digits of the given value. The value of the gravitational constant used to calculate the masses of Jupiter and Saturn is $G = 6.67259 \times 10^{-8}$ dyn · cm^2 · g^{-1} (Cohen & Taylor 1986).
[a]Campbell & Synott (1985).
[b]Campbell & Anderson (1989).
[c]Anderson et al. (1987).
[d]Tyler et al. (1989).
[e]Lindal et al. (1981).
[f]Lindal et al. (1985).
[g]Lindal (1992).
[h]From fourth-order figure theory.
[i]$(2R_{eq} + R_{pol})/3$ (Clairaut's approximation).
[j]Davies et al. (1986).
[k]Warwick et al. (1986).
[l]Warwick et al. (1989).

to the interior rotation. The giant planets are relatively fast rotators, with periods of approximately 10 h for Jupiter and Saturn and approximately 17 h for Uranus and Neptune. The fact that this fast rotation visibly affects the figure (shape) of these planets is seen by the significant difference between the polar and equatorial radii.

A first result obtained from the masses and radii (using the planets' mean radii, as defined in Section 2.7) indicated in Table 1 is the fact that these planets have low densities. These densities are similar, but considering that compression strongly increases with mass, one is led to a subclassification between the hydrogen-helium giant planets Jupiter and Saturn, and the ice giants Uranus and Neptune.

The values of the axial moment of inertia C have been calculated using the Radau-Darwin approximation (Zharkov & Trubitsyn 1978). Our four giant planets all have an axial moment of inertia substantially lower than the value for a sphere of uniform density, i.e., $2/5\, MR^2$, indicating that they have dense central regions. This does not necessarily mean that they possess a core, but simply that the density profile departs significantly from a uniform value.

TABLE 2 Energy balance as determined from Voyager IRIS data[a]

	Jupiter	Saturn	Uranus	Neptune
Absorbed power [10^{23} erg $\cdot$ s^{-1}]	50.14(248)	11.14(50)	0.526(37)	0.204(19)
Emitted power [10^{23} erg $\cdot$ s^{-1}]	83.65(84)	19.77(32)	0.560(11)	0.534(29)
Intrinsic power [10^{23} erg $\cdot$ s^{-1}]	33.5(26)	8.63(60)	0.034(38)	0.330(35)
Intrinsic flux [erg $\cdot$ s^{-1} $\cdot$ cm^{-2}]	5440.(430)	2010.(140)	42.(47)	433.(46)
Bond albedo	0.343(32)	0.342(30)	0.300(49)	0.290(67)
Effective temperature [K]	124.4(3)	95.0(4)	59.1(3)	59.3(8)
1-bar temperature[b] [K]	165.(5)	135.(5)	76.(2)	72.(2)

[a]After Pearl & Conrath (1991).
[b]Lindal (1992).

Jupiter, Saturn, and Neptune are observed to emit significantly more energy than they receive from the Sun (see Table 2). The case of Uranus is less clear. Its intrinsic heat flux $F_{\rm int}$ is significantly smaller than that of the other giant planets. Detailed modeling of its atmosphere, however, indicates that $F_{\rm int} \gtrsim 60\,{\rm erg\,cm^{-2}\,s^{-1}}$ (Marley & McKay 1999). With this caveat, all four giant planets can be said to emit more energy than they receive from the Sun. Hubbard (1968) showed, in the case of Jupiter, that this can be explained simply by the progressive contraction and cooling of the planets.

It should be noted that the 1 bar temperatures listed in Table 2 are retrieved from radio-occultation measurements using a helium to hydrogen ratio, which, at least in the case of Jupiter and Saturn, was shown to be incorrect. The new values of Y are found to lead to increased temperatures by $\sim$5 K in Jupiter and $\sim$10 K in Saturn (see Guillot 1999a). However, the *Galileo* probe found a 1 bar temperature of 166 K (Seiff et al. 1998) and generally a good agreement with the *Voyager* radio-occultation profile with the wrong He/H_2 value.

3.2. Atmospheric Composition

The most important components of the atmospheres of our giant planets are also among the most difficult to detect: H_2 and He have a zero dipolar moment. Also, their rotational lines are either weak or broad. On the other hand, lines owing to electronic transitions correspond to very high altitudes in the atmosphere and bear little information on the structure of the deeper levels. The only robust result concerning the abundance of helium in a giant planet is by in situ measurement by the *Galileo* probe in the atmosphere of Jupiter (von Zahn et al. 1998). The helium mole fraction (i.e., number of helium atoms over the total number of species in a given volume) is $q_{\rm He} = 0.1359 \pm 0.0027$. The helium mass mixing ratio Y (i.e., mass of helium atoms over total mass) is constrained by its ratio over hydrogen, X: $Y/(X+Y) = 0.238 \pm 0.05$. This ratio is by coincidence that found in the Sun's atmosphere, but because of helium sedimentation in the Sun's radiative zone, it

was larger in the protosolar nebula: $Y_{\text{proto}} = 0.275 \pm 0.01$ and $(X+Y)_{\text{proto}} \approx 0.98$. Less helium is therefore found in the atmosphere of Jupiter than inferred to be present when the planet formed.

Helium is also found to be depleted compared to the protosolar value in Saturn's atmosphere. However, in this case the analysis is complicated by the fact that *Voyager* radio occultations apparently led to a wrong value. The current adopted value is now $Y = 0.18 - 0.25$ (Conrath & Gautier 2000), in agreement with values predicted by interior and evolution models (Guillot 1999a, Hubbard et al. 1999). Finally, Uranus and Neptune are found to have near-protosolar helium mixing ratios, but with considerable uncertainty (Gautier & Owen 1989).

The abundance of heavy elements, i.e., elements other than hydrogen and helium, bears crucial information for the understanding of the processes that led to the formation of these planets. Again, the most precise measurements are for Jupiter, thanks to the *Galileo* probe. As shown by Figure 5, most of the heavy elements are enriched by a factor of two to four compared with the solar abundance (Niemann et al. 1998, Owen et al. 1999). One exception is neon, but an explanation is its capture by the falling helium droplets (Roulston & Stevenson 1995). Another exception is water, but this molecule is affected by meteorological processes, and the probe was shown to have fallen into a dry region of Jupiter's atmosphere. There are strong indications that its abundance is at least solar. Possible very high interior

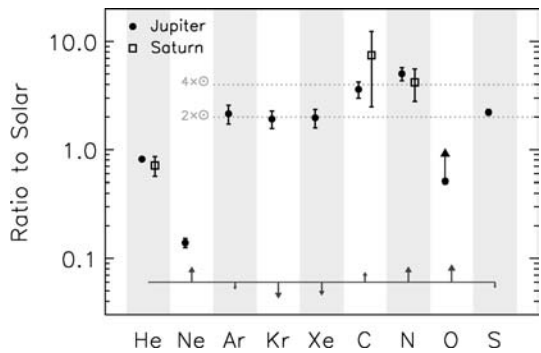

Figure 5 Elemental abundances measured in the tropospheres of Jupiter (*circles*) and Saturn (*squares*) in units of their abundances in the protosolar nebula. The elemental abundances for Jupiter are derived from the in situ measurements of the *Galileo* probe (e.g., Mahaffy et al. 2000, Atreya et al. 2003). Note that the oxygen abundance is considered to be a minimum value owing to meteorological effects (Roos-Serote et al. 2004). The abundances for Saturn are spectroscopic determination (Atreya et al. 2003 and references therein). The solar or protosolar abundances used as a reference are from Lodders (2003). The arrows show how abundances are affected by changing the reference protosolar abundances from those of Anders & Grevesse (1989) to those of Lodders (2003). The horizontal dotted lines indicate the locus of a uniform two and four times solar enrichment in all elements except helium and neon, respectively.

abundances (∼10 times the solar value) have also been suggested as a scenario to explain the delivery of heavy elements to the planet (Gautier et al. 2001, Hersant et al. 2004).

In the case of Saturn, both carbon in the form of methane and nitrogen as ammonia appear to be significantly enriched, but with large error bars (Atreya et al. 2003). In Uranus and Neptune, methane is probably between 30 and 60 times the solar value (Gautier & Owen 1989, Hersant et al. 2004).

3.3. Interior Models: Jupiter and Saturn

As illustrated by Figure 6, the simplest interior models of Jupiter and Saturn matching all observational constraints assume the presence of three main layers: (*a*) an outer hydrogen-helium envelope, whose global composition is that of the deep atmosphere; (*b*) an inner hydrogen-helium envelope, enriched in helium because the whole planet has to fit the H/He protosolar value; and (*c*) a central dense core. Because the planets are believed to be mostly convective, these regions are expected to be globally homogeneous. (Many interesting thermochemical transformations take place in the deep atmosphere, but they are of little concern to this review.)

A large part of the uncertainty in the models lies in the existence and location of an inhomogeneous region in which helium separates from hydrogen to form helium-rich droplets that fall deeper into the planet owing to their larger density. Models have generally assumed this region to be relatively narrow because helium was thought to be most insoluble in low-pressure metallic hydrogen (e.g., Stevenson 1982). However, DFT calculations have indicated that the critical

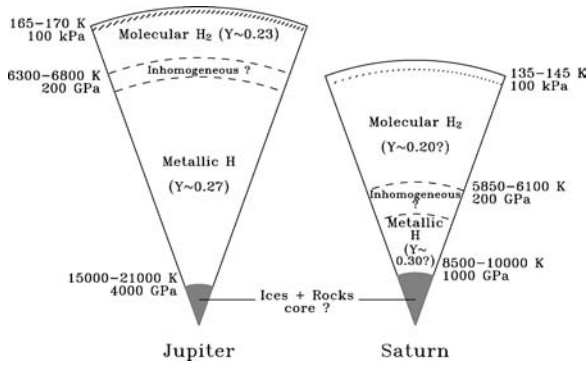

Figure 6 Schematic representation of the interiors of Jupiter and Saturn. The range of temperatures is estimated using homogeneous models and including a possible radiative zone indicated by the hashed regions. Helium mass mixing ratios *Y* are indicated. The size of the central rock and ice cores of Jupiter and Saturn is very uncertain (see text). In the case of Saturn, the inhomogeneous region may extend down all the way to the core, which would imply the formation of a helium core. Adapted from Guillot 1999b.

temperature for helium demixing may rise with pressure (Pfaffenzeller et al. 1995), presumably in the regime where hydrogen is only partially ionized and bound states remain. This opens up the possibility that the inhomogeneous regions may be more extended. In particular, in the case of Saturn, Fortney & Hubbard (2003) have shown that explaining Saturn's age may require that helium fall all the way to the core, thereby yielding the formation of a helium core (or of a helium shell around a rock or ice core).

With these caveats, the three-layer models can be used as a useful guidance to a necessarily hypothetical ensemble of allowed structures and compositions of Jupiter and Saturn. Figure 7 shows such an ensemble for Jupiter based on calculations by Saumon & Guillot (2004). The calculations assume that only helium is inhomogeneous in the envelope (the abundance of heavy elements is supposed to be uniform accross the molecular/metallic hydrogen transition). Many sources of uncertainties are included, however; among them, the most significant are on the EOS of hydrogen and helium, the uncertain values of J_4 and J_6, the presence of differential rotation deep inside the planet, the location of the helium-poor to helium-rich region, and the uncertain helium to hydrogen protosolar ratio.

These results show that Jupiter's core is smaller than $\sim$10 $M_\oplus$, and that its global composition is pretty much unknown (between 10 to 42 $M_\oplus$ of heavy elements in total). The models indicate that Jupiter is enriched compared to the solar value, particularly with the new, low value of $Z_\odot$ (Lodders 2003) used in Figure 7. This

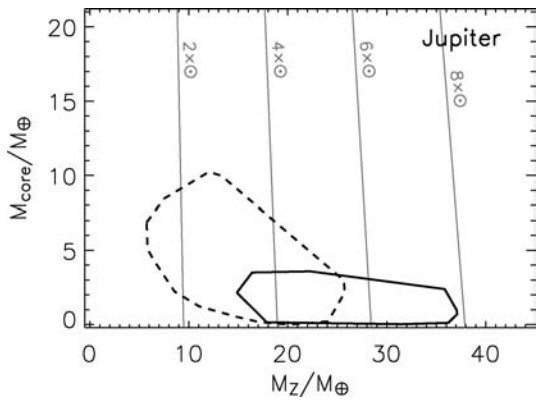

Figure 7 Constraints on Jupiter's interior structure based on Saumon & Guillot (2004). The value of the core mass ($M_{\rm core}$) is shown in function of the mass of heavy elements in the envelope (M_Z) for models matching all available observational constraints. The dashed region corresponds to models matching the laser compression experiments. The plain box corresponds to models matching the pulsed power and convergent shock compression experiments (see text). Grey lines indicate the values of M_Z that imply uniform enrichments of the envelope in heavy elements by factors of two to eight times the solar value ($Z_\odot = 0.0149$), respectively.

enrichment could be compatible with a global uniform enrichment of all species near the atmospheric *Galileo* values. Alternatively, species like oxygen (as mostly water) may be significantly enriched.

Most of the constraints are derived from the values of the radius (or equivalently mass) and of J_2. The measurement of J_4 allows to further narrow the ensemble of possible models, and in some cases, to rule out EOS solutions (in particular those indicating relatively large core masses, between 10 and 20 $M_\oplus$). As discussed in Guillot (1999a) and Saumon & Guillot (2004), most of the uncertainty in the solution arises because very different hydrogen EOSs are possible. The fact that more laboratory and numerical experiments seem to indicate relatively low compressions for hydrogen at Mbar pressures points toward smaller core masses and a larger amount of heavy elements in the planet (plain box in Figure 7). However, this relies on uncertain temperature gradients because the EOSs are based on laboratory data obtained at temperatures higher than those relevant to the planetary interiors.

Results slightly outside the boxes of Figure 7 are possible in the presence of a discontinuity of the abundance of heavy elements in the interior. Thus, Guillot (1999a) found slightly larger core masses (up to 12 $M_\oplus$) in the case of the Saumon-Chabrier EOS with a first-order plasma-phase transition.

In the case of Saturn (Figure 8), the solutions depend less on the hydrogen EOS because the Mbar pressure region is comparatively smaller. The total amount of heavy elements present in the planet can therefore be estimated with a better accuracy than for Jupiter. However, because Saturn's metallic region is deeper into the planet, it mimics the effect that a central core would have on J_2. If we allow for variations in the abundance of heavy elements together with the helium discontinuity, then the core mass can become much smaller, and even solutions with no core can be found (Guillot 1999a). These solutions depend on the hypothetic

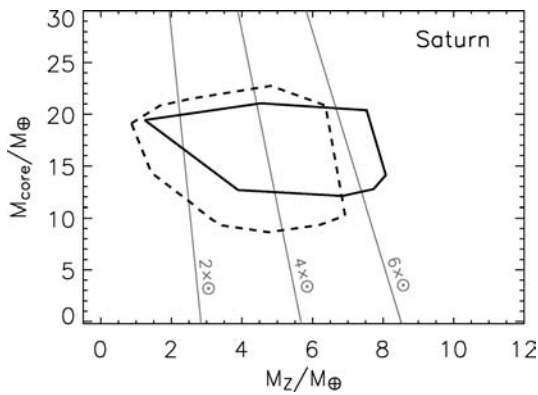

Figure 8 Same as Figure 7 in the case of Saturn. Note that smaller core masses could result either from allowing a variation of the abundance of heavy elements near the molecular/metallic transition (Guillot 1999a) or from the presence of a helium shell around the core (Fortney & Hubbard 2003).

phase separation of an abundant species (e.g., water), and generally cause an energy problem because of the release of considerable gravitational energy. However, another possibility is through the formation of an almost pure helium shell around the central core, which could lower the core masses by up to 7 $M_\oplus$ (Fortney & Hubbard 2003; W.B. Hubbard, personnal communication).

3.4. Interior Models: Uranus and Neptune

Although the two planets are relatively similar, Figure 3 already shows that Neptune's larger mean density compared to Uranus has to be due to a slightly different composition: either more heavy elements compared to hydrogen and helium or a larger rock/ice ratio. The gravitational moments impose that the density profiles lie close to that of ices (a mixture initially composed of H_2O, CH_4, and NH_3, but which rapidly becomes an ionic fluid of uncertain chemical composition in the planetary interior), except in the outermost layers, which have a density closer to that of hydrogen and helium (Marley et al. 1995, Podolak et al. 2000). As illustrated in Figure 9, three-layer models of Uranus and Neptune consisting of a central rock core (magnesium-silicate and iron material), an ice layer, and a hydrogen-helium gas envelope have been calculated (Podolak et al. 1991, Hubbard et al. 1995).

The fact that models of Uranus assuming homogeneity of each layer and adiabatic temperature profiles fail in reproducing its gravitational moments seems to imply that substantial parts of the planetary interior are not homogeneously mixed (Podolak et al. 1995). This could explain the fact that Uranus' heat flux is so small: Its heat would not be allowed to escape to space by convection but through a much slower diffusive process in the regions of high-molecular-weight gradient. Such regions would also be present in Neptune, but much deeper, thus allowing more heat to be transported outward. The existence of these nonhomogeneous, partially mixed regions are further confirmed by the fact that if hydrogen is supposed to be confined solely to the hydrogen-helium envelope, models predict ice/rock ratios of the order of 10 or more, much larger than the protosolar value of ∼2.5. On the other hand, if we impose the constraint that the ice/rock ratio is protosolar, the

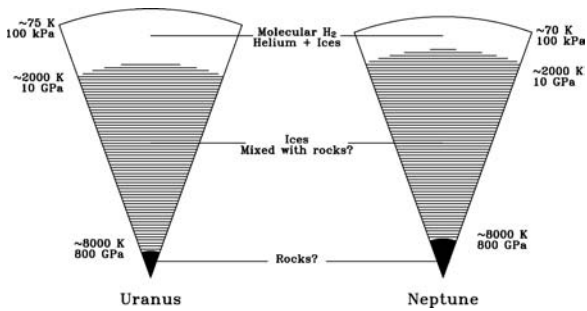

Figure 9 Schematic representation of the interiors of Uranus and Neptune. Adapted from Guillot 1999b.

overall composition of both Uranus and Neptune is, by mass, approximately 25% rocks, 60%–70% ices, and 5%–15% hydrogen and helium (Podolak et al. 1991, 1995; Hubbard et al. 1995). Assuming both ices and rocks are present in the envelope, an upper limit to the amount of hydrogen and helium present is $\sim$4.2 $M_\oplus$ for Uranus and $\sim$3.2 $M_\oplus$ for Neptune (Podolak et al. 2000). A lower limit of $\sim$0.5 $M_\oplus$ for both planets can be inferred by assuming that hydrogen and helium are only present in the outer envelope at $P \lesssim 100$ kbar.

3.5. Are the Interiors Adiabatic?

As discussed, the near-adiabaticity of the interiors of the giant planets is a consequence of the rapid rise of opacities with increasing pressure and temperatures. Several exceptions are possible:

(*a*) In the meteorological layer, the temperature gradient could become either subadiabatic (because of latent heat release and moist convection) or superadiabatic (because of molecular weight gradients created by condensation and precipitation). Locally, a depletion of an efficient radiative absorber (e.g., water or methane) could imply that convection is suppressed, either because of a lowered radiative gradient or because sunlight can then be deposited to this level. In Uranus and Neptune, a superadiabatic region at $P \sim 1$–2 bar is correlated with methane condensation (Lindal 1992, Guillot 1995). In Jupiter, the *Galileo* probe measured a nearly adiabatic profile, with a slight static stability ($N < 0.2\,\mathrm{K\,km^{-1}}$) down to 20 bars (Magalhães et al. 2002).

(*b*) At the PPT between molecular and metallic hydrogen, if it exists, with an entropy jump that could be of order 1 k_B/baryon (Stevenson & Salpeter 1977, Saumon et al. 1995).

(*c*) In the hydrogen-helium phase separation region, where a slow droplet formation may inhibit convection and yield a significant superadiabacity (Stevenson & Salpeter 1977).

(*d*) Near the core/envelope interface (whether it is abrupt or not), where an inhibiting molecular weight gradient occurs and, in the case of Jupiter, conduction might play a role.

(*e*) Throughout the planets, even though mixing-length arguments predict that the superadiabacity is extremely small ($\sim 10^{-6}$ or less), rotation and magnetic fields may increase it, although probably by modest amounts (Stevenson 1982; see also discussion in Guillot et al. 2004).

3.6. What Are the Ages of Our Giant Planets?

If we understand something of the formation of our Solar System and of other stars, our giant planets should have formed 4.55 Ga ago (e.g., Bodenheimer & Lin 2002). The model ages show significant deviations from that value, however.

In the case of Jupiter, the present radius and luminosity are obtained after 3.5 to 5.5 Ga of evolution, but most realistic EOSs predict ages above 4.5 Ga (Saumon & Guillot 2004). Several processes, including core erosion, could lead to a reduction of that value (Guillot et al. 2004). For Saturn, homogeneous evolution models predict ages of order 2 Ga (Stevenson 1982, Saumon et al. 1992, Guillot et al. 1995). In both planets, the presence of a phase separation of helium is likely and would tend to lengthen the cooling.

The case of Uranus and Neptune is less clear-cut because of the uncertainties both on the properties of their atmospheres (in particular their evolution with time) and on the global specific heat of material inside. It appears, however, that both planets have luminosities that are too small. This could be due to a cold start (relatively low initial temperatures), a rapid loss of the internal heat, or a strong molecular weight gradient that prevents interior regions from cooling (Podolak et al. 1991, Hubbard et al. 1995).

3.7. Do Some Elements Separate from Hydrogen at High Pressures? Where?

Helium is strongly suspected of separating from hydrogen in Jupiter and Saturn because its lower than protosolar abundance in the atmosphere, and in Saturn because without this additional energy source, the planet would evolve to its present state in $\sim$2 Ga. However, it has not been shown so far that a hydrogen helium mixture at Mbar pressures has a critical demixing temperature that is above that required in Jupiter and Saturn.

Helium demixing should occur in the metallic hydrogen region, but it is not clear that the critical temperature should decrease with pressure as for fully ionized plasmas (Stevenson 1982), or increase with pressure (Pfaffenzeller et al. 1995). The first scenario would imply the existence of a small inhomogeneous region near the molecular/metallic transition as illustrated in Figure 6. The second one would yield a more extended inhomogeneous region.

Evolution models including the two phase diagrams by Fortney & Hubbard (2003) show that to reconcile Saturn's age with that of the Solar System and the atmospheric helium abundance derived by Conrath & Gautier (2000), sufficient energy $\sim \Delta M_{\mathrm{He}} g H$ is required. This implies maximizing H, the distance of sedimentation of helium droplets, and hence favors the Pfaffenzeller-type phase diagram and the formation of a helium core.

The question of a phase separation of other elements is still open. It is generally regarded as unlikely at least in Jupiter and Saturn because of their small abudances relative to hydrogen and the fact that the critical demixing temperature depends exponentially on that abundance.

3.8. How Do the Planetary Interiors Rotate?

Interior rotation is important because it affects the gravitational moments and their interpretation in terms of density profiles (Zharkov & Trubitsyn 1978). It is

presently not known whether the observed atmospheric zonal flow patterns are tied to the planetary interiors or whether they are surface phenomena with the interior rotating close to a solid body with the rate given by the magnetic field. Interior rotation affects more significantly gravitational moments of higher order. Using extrema set by solid rotation and by a model in which the zonal wind pattern is projected into a cylindrical rotation (Hubbard 1982), one can show that interior rotation introduces an uncertainty equivalent to the present error bar for J_4, of the order of the spread in interior models for J_6, and that becomes dominant for J_8 and above. Measurements of high order gravitational moments J_8–J_{14} should tell whether atmospheric zonal flow penetrate into the deep interior or whether the deep rotation is mainly solid (Hubbard 1999).

3.9. What Can We Tell of the Giant Planets' Cores? Are They Primordial?

Confronted with diagrams such as Figures 6 and 9, there is the tendency to think of the giant planets' cores as well defined, separate entities. This is not necessarily the case: First, as shown by Figure 4, solutions with a well-defined central core are equivalent to solutions with cores that have been diluted into the central half of the planet. Second, convection does not necessarily guarantee the presence of globally homogeneous regions and can efficiently oppose the settling of species, as observed in thermohaline convection. Finally, the history of core formation, in particular the epoch at which planetesimals were accreted, and their sizes matter (e.g., Stevenson 1985).

Once formed, the cores of the giant planets are difficult to erode, as this demands both that heavy elements are (at least partially) soluble in the hydrogen helium envelope and that enough energy is present to overcome the molecular weight barrier that is created (Stevenson 1982). However, in the case of Jupiter at least, the second condition may not be that difficult to obtain, as only 10% of the energy in the first convective cell (in the sense of the mixing length approach) needs to be used to dredge up approximately $20\,M_\oplus$ of core material (Guillot et al. 2004). Evaluating whether the first condition is satisfied would require knowing the core's composition and its state, but one can nevertheless note that the initially high central temperatures ($\sim$30,000 K) favor solubility. Such an efficient erosion would not occur in Saturn (and much less so in Uranus and Neptune) because of its smaller total mass.

3.10. Do We Understand the Planets' Global Compositions?

This may be the hardest question because it requires tying all the different aspects of planet formation to the observations of the atmospheres of the giant planets and to the constraints on their interior structures. So far, most of the focus has been on explaining the presence of a central core of $\sim 10\,M_\oplus$ in Jupiter, Saturn, Uranus, and Neptune. The new interior data suggest that Jupiter's core is probably smaller and that Saturn's may be larger. More importantly, the envelopes of all

planets appear to be enriched in heavy elements, and this has to be explained as well.

The possibility that Jupiter could have been formed by a direct gravitational instability (e.g., Boss 2000) may be appealing in view of its small inferred core. However, the enrichment of its envelope in heavy elements is difficult to explain within that scenario given the low accretion rate of a fully formed Jupiter (Guillot & Gladman 2000).

The leading scenario therefore remains the standard core accretion scenario (Pollack et al. 1996), with the addition that Jupiter, Saturn, Uranus, and Neptune were closer together (5–20 AU) just after their formation (Levison & Morbidelli 2003). Although this scenario requires core masses $\gtrsim 10\,M_\oplus$, the possibility of an erosion of Jupiter's core is appealing because it would both explain the difference in size with Saturn and an enrichment of its envelope. Although more limited, a small $\sim 2\,M_\oplus$ erosion of Saturn's core could provide part of the enrichment of the envelope (Guillot et al. 2004).

The fact that Jupiter's atmosphere is also enriched in noble gases, in particular Ar, which condenses at very low temperatures (~ 30 K), is still a puzzle. Presently invoked explanations include a clathration of noble gases in ices (Gautier et al. 2001, Hersant et al. 2004) and the delivery of planetesimals formed at very low temperatures (Owen et al. 1999).

Finally, the large enrichments in C and possibly N of the atmospheres of Uranus and Neptune probably indicate that a significant mass of planetesimals ($\gtrsim 0.1\,M_\oplus$) impacted the planets after they had captured most of their present hydrogen-helium envelopes. Along with the other problems related to this section, this requires quantitative work.

4. EXTRASOLAR PLANETS

4.1. Observables

More than 145 extrasolar planets have been discovered to date (see J. Schneider's *Extrasolar Planets Encyclopedia* on http://www.obspm.fr/planets), but only those for which a determination of both the planetary mass and radius are useful for the purposes of this review. This can only be done for planets that transit in front of their star, which, by probabilistic arguments, limits us to planets that orbit close to their star. I am therefore only concerned with Pegasi planets, giant planets similar to 51 Peg b and HD209458b (both in the constellation Pegasus), with semi-major axes smaller than 0.1 AU.

Six transiting Pegasi planets have been discovered to date. Their main characteristics are listed in Table 3. The first one, HD209458b (Charbonneau et al. 2000, Henry et al. 2000), has been shown to possess sodium in its atmosphere (Charbonneau et al. 2002) and to have an extended, evaporating atmosphere (Vidal-Madjar et al. 2003, 2004). Four others have been discovered by the photometric OGLE survey and subsequent radial velocity measurements (Konacki et al. 2003,

TABLE 3 Systems with transiting Pegasi planets discovered to date

	Age [Ga]	[Fe/H]	a [AU]	$T^{\star}_{\rm eq}$ [K]	$M_{\rm p}/M_{\rm J}$	$R_{\rm p}/10^{10}$ cm
HD209458[a]	4–7	0.00(2)	0.0462(20)	1460(120)	0.69(2)	1.02(9)
OGLE-56[b]	2–4	0.0(3)	0.0225(4)	1990(140)	1.45(23)	0.88(11)
OGLE-113[c]	?	0.14(14)	0.0228(6)	1330(80)	0.765(25)	$0.77\binom{+5}{-4}$
OGLE-132[d]	0–1.4	0.43(18)	0.0307(5)	2110(150)	1.19(13)	0.81(6)
OGLE-111[e]	?	0.12(28)	0.0470(10)	1040(160)	0.53(11)	$0.71\binom{+9}{-4}$
TrES-1[f]	?	0.00(4)	0.0393(11)	1180(140)	0.75(7)	0.77(4)

⋆Equilibrium temperature calculated on the basis of a zero planetary albedo.
[a]Brown et al. (2001), Cody & Sasselov (2002).
[b]Konacki et al. (2003), Sasselov (2003), Torres et al. (2004).
[c]Bouchy et al. (2004), Konacki et al. (2004).
[d]Moutou et al. (2004).
[e]Pont et al. (2004).
[f]Alonso et al. (2004), Laughlin et al. (2004), Sozzetti et al. (2004).

2004; Bouchy et al. 2004; Pont et al. 2004). One is a result of the TrES network survey (Alonso et al. 2004). Present photometric surveys have a strong detection bias toward very short periods that are associated to a probability of transiting that is inversely proportional to the orbital distance, which shows that Table 3 represents only a tiny fraction of planets that may have a low probability of existence.

A crucial parameter for the evolution models is the equilibrium temperature $T_{\rm eq} = T_* \sqrt{R_*/2a}$ (assuming a zero albedo, i.e., that all incoming stellar light is absorbed by the planetary atmosphere). With values of $T_{\rm eq}$ between ∼1000 and 2000 K, the present sample of transiting planets is already quite rich.

4.2. Observed Versus Calculated Radii of Pegasi Planets

Contrary to the giant planets in our Solar System, Pegasi planets are subject to an irradiation from their central star that is so intense that the absorbed stellar energy flux is approximately 10^4 times larger than their intrinsic flux (estimated from Equation 9, or calculated directly). The atmosphere is thus prevented from cooling, with the consequence that a radiative zone develops and governs the cooling and contraction of the interior (Guillot et al. 1996). Typically, for a planet like HD209458b, this radiative zone extends to kbar levels, $T \sim 4000$ K, and is located in the outer 5% in radius (0.3% in mass) (Guillot & Showman 2002).

Problems in the modeling of the evolution of Pegasi planets arise mostly because of the uncertain outer boundary condition. The intense stellar flux implies that the atmospheric temperature profile is extremely dependant on the opacity sources considered. Depending on the chosen composition, the opacity data used, the assumed presence of clouds, and the geometry considered, resulting temperatures in the deep atmosphere can differ by up to ∼600 K (Seager & Sasselov 1998, 2000; Goukenleuque et al. 2000; Barman et al. 2001; Sudarsky et al. 2003; Iro

et al. 2004). Because of this problem, and in the framework of our simple model, the following discussion is based on an outer boundary condition at 1 bar and a fixed temperature $T_1 = 1500$ or 2000 K.[1]

Another related problem is the presence of the radiative zone. Again, the composition is unknown and the opacity data are uncertain in this relatively high temperature ($T \sim 1500$–3000 K) and high pressure (up to ~1 kbar) regime. Results from our models are based on opacities from Allard et al. (2001). Other calculations using, e.g., the widely used Alexander & Ferguson (1994) opacities, do yield only a slightly faster cooling, even though the Rosseland opacities are lower by a factor ~3 in this regime.

The resulting mass-radius relations are shown in Figure 10 for $T_1 = 1500$ and 2000 K and compared with the observations for the planets listed in Table 3. For each case, an upper limit on the radius is obtained from a pure hydrogen-helium composition with $Y = 0.25$. An ad hoc lower limit comes from a model with a $15\,M_\oplus$ central core, and a $Y = 0.30$ envelope. In both cases, the opacity table is unchanged.

Figure 10 shows that within uncertainties, the measurements for four out of six planets can be explained in the framework of our simple model. However, two cases stand out: OGLE-TR-132b appears too small for its age, implying that it may contain significant amounts of heavy elements in a core or in its deep interior. The case of HD209458b is more problematic: The constraints on its age, mass, and deep atmospheric temperature that should be ~1500–2000 K yield radii that are approximately 10% to 20% smaller than measured (Bodenheimer et al. 2001, 2003; Guillot & Showman 2002; Baraffe et al. 2003). The fact that the measured radius corresponds to a low-pressure (~mbar) level, whereas the calculated radius corresponds to a level near 1 bar is not negligible (Burrows et al. 2004) but too small to account for the difference. This is problematic because although it is easy to invoke the presence of a massive core to explain the small size of a planet, a large size such as that of HD209458b may require an additional energy source.

Bodenheimer et al. (2001) proposed that this large radius may be due to a small forced eccentricity ($e \sim 0.03$) of HD209458b, and subsequent tidal dissipation in the planet interior. In this case, $\dot{\epsilon} > 0$ in the energy conservation equation (Equation 4). Because of the relatively limited amount of energy available in the (noncircular) orbit and the presumably rapid dissipation (owing to a tidal Q that is presumably similar to that of Jupiter, i.e., $Q \sim 10^5$–10^6), this requires the presence of an unseen eccentric companion. The search for this companion and a possible nonzero eccentricity of HD209458b is ongoing (Bodenheimer et al. 2003).

[1]Technically, to obtain high entropy initial conditions I use $T_1 \sim T_{\rm eq}(1 + L/L_{\rm eq})^{1/4}$, but the precise form does not matter as long as $L \ll L_{\rm eq}$, or equivalently $-T_1 dS_1/dt \ll -T_{\rm int} dS_{\rm int}/dt$, where $S_{\rm int}$ is the characteristic interior entropy. The equality between T_1 and $T_{\rm eq}$ is only a very rough estimate guided by present works on atmospheric models of heavily irradiated planets.

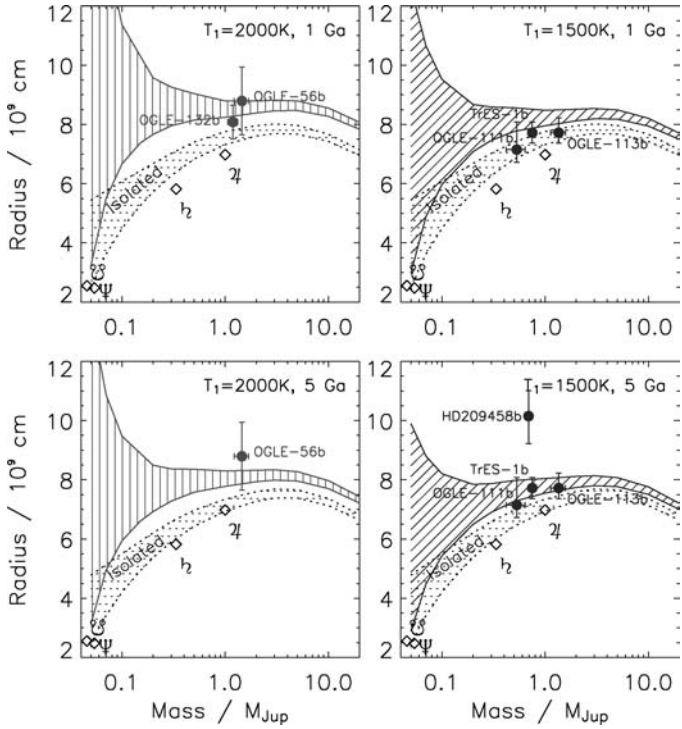

Figure 10 Mass-radius relation of strongly irradiated planets with ages of 1 Ga (*upper panels*) and 5 Ga (*lower panels*), and 1-bar temperatures equal to 2000 (*left panels*) and 1500 K (*right panels*), respectively. The hashed areas have upper and lower envelopes defined by ($Y = 0.25$, $M_{\rm core} = 0$) and ($Y = 0.30$, $M_{\rm core} = 15\,M_\oplus$), respectively. Dotted symbols with error bars indicate known objects, plotted as a function of their estimated 1-bar temperatures and ages. Planets whose age is uncertain appear in both upper and lower panels. Solution for nonirradiated planets (*dotted lines*) are shown for easier comparison.

A natural possibility may be the stellar flux itself because transporting to deep levels (∼100 bars or more) only a small fraction of order 0.1% to 1% of the incoming flux would yield a radius that is in agreement with the observations. On this basis, Showman & Guillot (2002) proposed that kinetic energy generated in the atmosphere owing to the strong asymmetry in stellar insolation may be transported to deep levels and dissipated there, possibly owing to a small asynchronous rotation and its dissipation by stellar tides. Another possibility evoked by the authors is that kilometer per second atmospheric winds may maintain the atmosphere into a shear-unstable, quasi-adiabatic state, which would force temperatures in excess of 3000 K at levels between ten and a few tens of bars.

It is puzzling that all other recently announced transiting planets do not require an additional energy source to explain their size: This is seen in Figure 10, which

shows that all planets except HD209458b are consistent with the evolutionary tracks.

Is there a consistent scenario explaining all the observations? One possibility is that, as proposed by Bodenheimer et al. (2001), HD209458b indeed has an eccentric companion. A second possibility is that their orbital histories have been very different. Finally, the planets may well have different compositions.

4.3. How Do Tides and Orbital Evolution Affect the Contraction and Cooling of Pegasi Planets?

The small orbital eccentricities of Pegasi planets compared with more distant extrasolar planets tell us that tides raised by the star on the planet have probably played an important role in circularizing their orbits, with a timescale estimated at ∼1 Ga for a planet at 0.05 AU (Rasio et al. 1996, Marcy et al. 1997). Synchronization is expected to occur in only Ma timescales (Guillot et al. 1996), maybe much less (Lubow et al. 1997). The tides raised by the planet on the star also tend to spin up the star, which leads to a decay of the planetary orbit. It is interesting to note that, with periods of only ∼1 day, the three OGLE planets lie close to the orbital stability threshold (Rasio et al. 1996) or would be predicted to fall into the star in Ga timescales or less (Witte & Savonije 2002, Pätzold & Rauer 2002).

The energies available from circularization and synchronization can be usefully compared to the gravitational energy of the planet (e.g., Bodenheimer et al. 2001, Showman & Guillot 2002):

$$E_{\rm circ} = \frac{e^2 G M_* M}{a} = 3.6 \times 10^{42} \left(\frac{e}{0.1}\right)^2 \left(\frac{M_*}{\rm M_\odot}\right) \left(\frac{M}{\rm M_J}\right) \left(\frac{a}{10 \rm R_\odot}\right)^{-1} \text{erg}, \quad (16)$$

$$E_{\rm sync} = \frac{1}{2} k^2 M R^2 \Delta\omega^2 = 2.4 \times 10^{41} \left(\frac{k^2}{0.25}\right) \left(\frac{M}{\rm M_J}\right) \times \left(\frac{R}{10^{10}\,\text{cm}}\right)^2 \left(\frac{\Delta\omega}{10^{-4}\,\text{s}^{-1}}\right)^2 \text{erg}, \quad (17)$$

$$E_{\rm grav} = \delta \frac{G M^2}{R} = 2.4 \times 10^{42} \left(\frac{\delta}{0.1}\right) \left(\frac{M}{\rm M_J}\right)^2 \left(\frac{R}{10^{10}\,\text{cm}}\right)^{-1} \text{erg}, \quad (18)$$

where e is the initial eccentricity, a is the planet's orbital distance, M is its mass, R is its radius, k is the dimensionless radius of gyration, $\Delta\omega$ is the change in the planet's spin before and after synchronization, and δ is approximately the change in the planet's radius (neglecting any structural changes in the calculation of $E_{\rm sync}$ and $E_{\rm grav}$). $E_{\rm grav}$ is the gravitational energy lost by the planet when its radius decreases by a factor $\sim\delta$, or, alternatively, the minimum energy required to expand its radius by the same factor.

The fact that the three energy sources are comparable implies that very early in the evolution, circularization and synchronization may have played a role, perhaps inducing mass loss (Gu et al. 2004). Once a planet has contracted to a degenerate,

low θ state, the gravitational energy becomes large, and circularization and synchronization only have a limited role to play. However, two reservoirs can be invoked: the orbital energy of a massive eccentric planet that would force a non-zero eccentricity of the inner one (Bodenheimer et al. 2001) and the absorbed stellar luminosity in its ability to create kinetic energy in the atmosphere (Showman & Guillot 2002).

A major uncertainty related to these processes and how they affect the planetary structure is to know how and where energy is dissipated. Lubow et al. (1997) proposed that a resonant tidal torque is exerted at the outer boundary of the inner convection zone and that dissipation occurs through the damping of gravity waves propagating in the outer stable radiative region. Contrary to Jupiter, this may be an efficient process because Pegasi planets have a radiative region that extends to great depths. Another possibility is through the excitation of inertial waves in the convective region, a process that would occur also in our giant planets (Ogilvie & Lin 2004). The location of the dissipation is not clear, however. If it occurs in the atmosphere, the effect of tides on the evolution will be limited, whereas they will have a maximum impact if they occur deep into the radiative zone (Guillot & Showman 2002).

If dissipation cannot reach into the deep interior, the planets will not inflate significantly when they migrate to their present location. This would imply that HD209458b must have migrated from several AUs to its present location in less than $\sim$10 Ma (Burrows et al. 2000b). In this framework, one could invoke a late migration of the OGLE planets (in particular OGLE-TR-132b) to explain their relatively small radius compared to HD209458b.

4.4. How Does the Composition Affect the Structure and Evolution?

It is generally believed that giant planets of the mass of Jupiter should have near-solar composition and relatively small core masses. However, it may not be the case: First, Jupiter is in fact relatively significantly enriched in heavy elements. Second, although Jupiter is very efficient at ejecting planetesimals from the Solar System, Pegasi planets are unable to do so because the local orbital speed $(GM_*/a)^{1/2}$ $\sim 150\,\mathrm{km\,s^{-1}}$ is much larger than the planet's escape velocity $(2GM/R)^{1/2}$ $\sim 50\,\mathrm{km\,s^{-1}}$ (Guillot & Gladman 2000). Furthermore, most planetesimals on low e orbits close to the planet would end up impacting the planet, not the star (A. Morbidelli, personal communication, 2004). For this reason, models of in situ formation of Pegasi planets generally yield large core masses $\sim$40 $M_\oplus$ (Bodenheimer et al. 2000). Pegasi planets should therefore be expected to have very different compositions and core masses, depending on the properties of the disk of planetesimals at their formation, the presence of other planets, and their orbital evolution.

The presence of a core has a relatively straightforward impact on the evolution of giants planets. As shown in Figure 10, it leads to a much faster contraction and a smaller radius at any given age. An enrichment of the envelope both increases

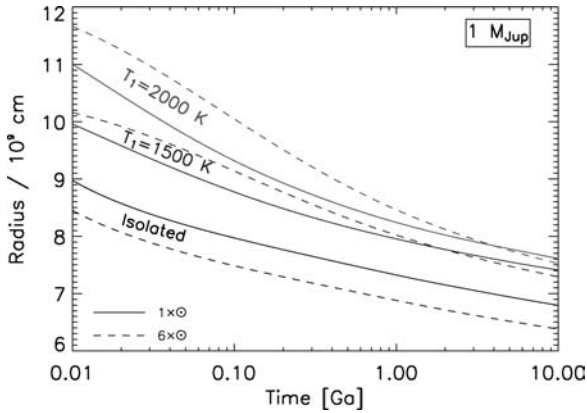

Figure 11 Evolution of giant planets in terms of radius versus time for different irradiation levels and two assumed compositions: solar and six times solar. (This calculation ignores second-order effects as modifications of the adiabatic temperature gradient and nonlinear effects in the opacity calculation, and more importantly modifications of atmospheric properties.)

the mean molecular weight and the opacities, with two opposite effects in terms of the planet's contraction and cooling. Figure 11 shows that for large irradiations (extended radiative zones), the second effect wins and leads to a (limited) increase of the planetary radius. However, planets with a larger mean molecular weight eventually become smaller.

The difference in inferred radii between HD209458b and other transiting planets could hence indicate that stellar tides play a role in slowing or even stalling the contraction of all planets, but because of different histories, some planets have a large core mass, but HD209458b does not. In that framework, OGLE-TR-132b would probably need a core of $\sim$20 $M_\oplus$ or more (or the same amount of heavy elements in its deep interior) to explain its small radius. The large [Fe/H] value measured for its parent star (Table 3) is an indication that the planet may indeed have grown a large core.

4.5. What Is the Role of the Atmosphere for the Evolution?

I have purposely used a very simple atmospheric model by setting $T_1 \propto T_{\rm eq} = {\rm cte}$. Of course, this hides many important complications, such as opacities, chemistry, gravity dependance, presence of clouds, atmospheric dynamics, dependance on the incoming stellar flux, etc. These complications partially explain differences between the findings of several authors (Seager & Sasselov 1998, 2000; Goukenleuque et al. 2000; Barman et al. 2001; Sudarsky et al. 2003; Iro et al. 2004). These works yield characteristic temperatures at the base of the atmosphere (i.e., where most of the incoming flux has been absorbed) that range from $\sim$1700 to $\sim$2300 K.

However, the largest differences arise from simple geometrical reasons: Because these calculations are one-dimensional, some authors choose to model the atmosphere at the substellar point, some average the received stellar flux over the day-hemisphere (1/2 less flux), and others average it over the entire planet (1/4 less flux). This points to real problems: How does the planet react to this extremely inhomogeneous stellar irradiation, and how do possible inhomogeneities in the atmosphere affect the planetary evolution?

Without atmospheric dynamics, a synchronous Pegasi planet at $\sim$0.05 AU of a G-type star would see its substellar point heated to $\sim$2500 K or more, and its night hemisphere and poles would have temperatures $\sim$100 K, a clearly unstable situation. Assuming synchronization of the convective interior and a radiative atmosphere obeying the Richardson shear-instability criterion, Showman & Guillot (2002) showed that the atmosphere of Pegasi planets are likely to develop kilometer per second winds, but that spatial photospheric temperature variations of $\sim$500 K are likely. Dynamical models using shallow-water equations by Cho et al. (2003) also yield latitudinal temperature variations, but predict a surprising time-dependent behavior, with a night-side that sometimes becomes hotter than the day side. A time-dependant approach of radiative transfer, in which the atmosphere is allowed to react to a varying irradiation, shows that a kilometer per second rotation indeed yields a $\sim$500 K effective temperature variation. It also shows that the conditions required for the shallow-water treatment (a relatively long radiative timescale) are probably not met in Pegasi planets (Iro et al. 2004).

As shown by Guillot & Showman (2002), to first order (i.e., neglecting possible nonlinear behavior due to, e.g., opacity temperature dependances and/or cloud formation), the cooling with an inhomogeneous boundary condition is faster than if the same amount of heat has been homogeneously distributed. This is because heat tends to escape more rapidly in regions of low atmospheric temperatures. But because the radiative timescale below optical depth unity is approximately $\propto P^2$, levels deeper than a few bars tend to homogenize horizontally very efficiently, even with a slow circulation (Iro et al. 2004).

Therefore, there is presently no reason to use for evolution models an atmospheric boundary condition other than that obtained assuming a stellar flux averaged over the entire planet. Of course, more work needs to be done, as opacity variations, the presence of clouds either on the day or night side (depending on the kind of circulation), nonequilibrium chemistry, and possible shear instabilities and gravity waves damping can all play an important role.

4.6. Stability and Evaporation?

Because Pegasi planets are so close to their star, the question of their survival has been among the first asked following the discovery of 51 Peg B. Guillot et al. (1996) and Lin et al. (1996) independently concluded a relatively fast contraction of the planet and its survival based on nonthermal evaporation rates extrapolated from Jupiter. These evaporation rates $\sim 10^{-16}\,M_\odot\,a^{-1}$ turn out to be extremely

close to those inferred from observations of HD209458b showing the escape of HI (Vidal-Madjar et al. 2003), OI, and CII (Vidal-Madjar et al. 2004). However, the atmospheric escape problem is more complex than initially envisioned, with XUV heating, conduction, and gravity waves playing important roles (Lammer et al. 2003, Lecavelier des Etangs et al. 2004).

Generally, a critical question is that of the stability of planets at close orbital distances in their young ages (Baraffe et al. 2004, Gu et al. 2004). Figure 11 shows that the cooling timescale is initially relatively long in the case of intense irradiation (see also figure 2 of Guillot et al. 1996) and might lead to a significant mass loss in case of a rapid inward migration because of Roche lobe overflow (part of the planetary envelope becomes unbound because of the star's gravitational potential) (Trilling et al. 1998, 2002). Baraffe et al. (2004) find that another route may be the strong exospheric evaporation. Below a critical mass, the planet would inflate before it can become degenerate enough. However, either the presence of a core and the consequent rapid contraction (see Figure 10), or an internal cooling associated to the decompression upon mass loss may protect the planets from an exponential evaporation.

5. CONCLUSION AND PROSPECTS

We are just beginning to discover the diversity of giant planets. Already, a variety of problems particular to one planet or a small ensemble of planets have arisen. Given the limited ensemble of objects that we are given to study and the rapid evolution of the subject, any attempt to find general rules is fraught with risk. Some salient conclusions should, however, resist the trial of time:

- The giant planets of our Solar System all contain a minimum of $10\,M_\oplus$ of heavy elements, and even $\sim 20\,M_\oplus$ for Saturn and probably Jupiter. In Jupiter, most of the heavy elements are mixed in the hydrogen-helium envelope. On the contrary, Saturn, Uranus, and Neptune appear to be significantly differentiated.
- The envelopes of Jupiter, Saturn, Uranus, and Neptune are enriched in heavy elements compared to a solar composition, implying that heavy elements were delivered either after the formation (requiring large masses in planetesimals because of the low accretion probabilities) or when the planets, and in particular Jupiter, were not fully formed. In that case, an upward mixing (erosion) of these elements with the envelope is required. A third possibility is that these elements were captured in an enriched nebula.
- The demixing of helium in metallic hydrogen has probably begun in Jupiter, and has been present in Saturn for 2–3 Ga.
- Like Jupiter and Saturn, the Pegasi planets discovered so far are mostly made of hydrogen and helium, but their precise composition depends on how tidal effects lead to the dissipation of heat in their interior.

Improvements in our knowledge of the giant planets requires a variety of efforts. Fortunately, nearly all of these are addressed at least partially by adequate projects in the next few years. The efforts that are necessary thus include (but are not limited to) the following:

- Obtain a better EOS of hydrogen, in particular, near the molecular/metallic transition. This will be addressed by the construction of powerful lasers, such as the NIF in the United States and the MégaJoule laser in France, and by innovative experiments such as shocks on precompressed samples. One of the challenges is not only obtaining higher pressures but mostly lower temperatures than currently possible with single shocks. The parallel improvement of computing facilities should allow more extended numerical experiments.
- Calculate hydrogen-helium and hydrogen-water phase diagrams. (Other phase diagrams are desirable too, but of lesser immediate importance.) This should be possible with new numerical experiments.
- Have a better yardstick to measure solar and protosolar compositions. This may be addressed by the analysis of the *Genesis* mission samples or may require another future mission.
- Improve the values of J_4 and J_6 for Saturn. This will be done as part of the *Cassini-Huygens* mission. This should lead to better constraints, and possibly a determination of whether the interior of Saturn rotates as a solid body.
- Detect new transiting extrasolar planets, and hopefully some that are further from their star. The space missions COROT (2006) and *Kepler* (2007) should provide the detection and characterization of many tens, possibly hundreds, of giant planets.
- Improve the measurement of Jupiter's gravity field and determine the abundance of water in the deep atmosphere. This would be possible either from an orbiter or even with a single fly-by (Bolton et al. 2003).

Clearly, there is a lot of work to be done, but the prospects for a much improved knowledge of giant planets and their formation are bright.

ACKNOWLEDGMENTS

It is a pleasure to thank Didier Saumon, Daniel Gautier, Doug Lin, Jonathan Fortney, Adam Showman, Bruno Bézard, Travis Barman, Brett Gladman, Christophe Sotin, and Scott Bolton for instructive discussions, and France Allard, Russ Hemley, Bill Hubbard and Alessandro Morbidelli for furthermore sharing new or unpublished results. This work was supported by CNRS and the Programme National de Planétologie.

LITERATURE CITED

Alexander DR, Ferguson JW. 1994. Low-temperature Rosseland opacities. *Ap. J.* 437: 879–91

Allard F, Hauschildt PH, Alexander DR, Tamanai A, Schweitzer A. 2001. The limiting effects of dust in brown dwarf model atmospheres. *Ap. J.* 556:357–72

Alonso R, Brown TM, Torres G, Latham DW, Sozzetti A, et al. 2004. TrES-1: The transiting planet of a bright K0 V star. *Ap. J.* 613:L153

Anders E, Grevesse N. 1989. Abundances of the elements—meteoritic and solar. *Geochem. Cosmo. Acta* 53:197–214

Anderson JD, Campbell JK, Jacobson RA, Sweetnam DN, Taylor AH. 1987. Radio science with Voyager 2 at Uranus—results on masses and densities of the planet and five principal satellites. *J. Geophys. Res.* 92: 14877–83

Atreya SK, Mahaffy PR, Niemann HB, Wong MH, Owen TC. 2003. Composition and origin of the atmosphere of Jupiter—an update, and implications for the extrasolar giant planets. *Planet. Space Sci.* 51:105–12

Baraffe I, Chabrier G, Barman TS, Allard F, Hauschildt P. 2003. Evolutionary models for cool brown dwarfs and extrasolar giant planets. The case of HD 209458. *Astron. Astrophys.* 402:701–12

Baraffe I, Selsis F, Chabrier G, Barman TS, Allard F, et al. 2004. The effect of evaporation on the evolution of close-in giant planets. *Astron. Astrophys.* 419:L13–16

Barman T, Hauschildt PH, Allard F. 2001. Irradiated planets. *Ap. J.* 556:885–95

Belov SI, Boriskov GV, Bykov AI, Il'kaev IL, Luk'yanov NB, et al. 2002. Shock compression of solid deuterium. *Sov. Phys. JETP Lett.* 76:433–35

Bodenheimer P, Hubickyj O, Lissauer JJ. 2000. Models of the in situ formation of detected extrasolar giant planets. *Icarus* 143:2–14

Bodenheimer P, Laughlin G, Lin DNC. 2003. On the radii of extrasolar giant planets. *Ap. J.* 592:555–63

Bodenheimer P, Lin DNC. 2002. Implications of extrasolar planets for understanding planet formation. *Annu. Rev. Earth Planet. Sci.* 30: 113–48

Bodenheimer P, Lin DNC, Mardling R. 2001. On the tidal inflation of short-period extrasolar planets. *Ap. J.* 548:466–72

Bolton SJ, Allison M, Anderson J, Atreya S, Bagenal F, et al. 2003. A polar orbiter to probe Jupiter's deep atmosphere, interior structure and polar magnetosphere. *DPS Meet.* 35:41.08

Bonev SA, Militzer B, Galli G. 2004. Ab initio simulations of dense liquid deuterium: comparison with gas-gun shock-wave experiments. *Phys. Rev. B* 69:014101

Boriskov GV, Bykov AI, Il'kaev IL, Selemir VD, Simakov GV, et al. 2003. Shock-wave compression of solid deuterium at a pressure of 120 GPa. *Dokl. Phys.* 48:553–55

Boss AP. 2000. Possible rapid gas giant planet formation in the solar nebula and other protoplanetary disks. *Ap. J.* 536:L101–4

Bouchy F, Pont F, Santos NC, Melo C, Mayor M, et al. 2004. Two new "very hot Jupiters" among the OGLE transiting candidates. *Astron. Astrophys.* 421:L13–16

Brown TM, Charbonneau D, Gilliland RL, Noyes RW, Burrows A. 2001. Hubble Space Telescope time-series photometry of the transiting planet of HD 209458. *Ap. J.* 552:699–709

Burrows A, Guillot T, Hubbard WB, Marley MS, Saumon D, et al. 2000b. On the radii of close-in giant planets. *Ap. J. Lett.* 534:L97–100

Burrows A, Hubeny I, Hubbard WB, Sudarsky D, Fortney JJ. 2004. Theoretical radii of

transiting giant planets: the case of OGLE-TR-56b. *Ap. J.* 610:L53–56

Burrows A, Marley MS, Sharp CM. 2000a. The near-infrared and optical spectra of methane dwarfs and brown dwarfs. *Ap. J.* 531:438–46

Campbell JK, Anderson JD. 1989. Gravity field of the Saturnian system from Pioneer and Voyager tracking data. *Astron. J.* 97:1485–95

Campbell JK, Synnott SP. 1985. Gravity field of the Jovian system from Pioneer and Voyager tracking data. *Astron. J.* 90:364–72

Cavazzoni C, Chiarotti GL, Scandolo S, Tosatti E, Bernasconi M, Parrinello M. 1999. Superionic and metallic states of water and ammonia at giant planet conditions. *Science* 283:44–46

Chandrasekhar S. 1939. *Stellar Structure and Evolution*. Chicago: Univ. Chicago Press

Charbonneau D, Brown TM, Latham DW, Mayor M. 2000. Detection of planetary transits across a Sun-like star. *Ap. J.* 529:L45–48

Charbonneau D, Brown TM, Noyes RW, Gilliland RL. 2002. Detection of an extrasolar planet atmosphere. *Ap. J.* 568:377–84

Cho JYK, Menou K, Hansen BMS, Seager S. 2003. The changing face of the extrasolar giant planet HD 209458b. *Ap. J.* 587:L117–20

Cody AM, Sasselov DD. 2002. HD 209458: Physical parameters of the parent star and the transiting planet. *Ap. J.* 569:451–58

Cohen ER, Taylor BN. 1986. The 1986 adjustment of the fundamental physical constants. *Rev. Mod. Phys.* 59:1121

Collins GW, da Silva LB, Celliers P, Gold DM, Foord ME, et al. 1998. Measurements of the equation of state of deuterium at the fluid insulator-metal transition. *Science* 281:1178–81

Conrath BJ, Gautier D. 2000. Saturn helium abundance: A reanalysis of Voyager measurements. *Icarus* 144:124–34

da Silva LB, Celliers P, Collins GW, Budil KS, Holmes NC, et al. 1997. Absolute equation of state measurements on shocked liquid deuterium up to 200 GPa (2 Mbar). *Phys. Rev. Lett.* 78:483–86

Datchi F, Loubeyre P, Letoullec R. 2000. Extended and accurate determination of the melting curves of argon, helium, ice (H_2O), and hydrogen (H_2). *Phys. Rev. B* 61:6535–46

Davies ME, Abalakin VK, Bursa M, Lederle T, Lieske JH, et al. 1986. Report of the IAUIAG COSPAR working group on cartographic coordinates and rotational elements of the planets and satellites: 1985. *Celest. Mech.* 39:102–13

Desjarlais MP. 2003. Density-functional calculations of the liquid deuterium Hugoniot, reshock, and reverberation timing. *Phys. Rev. B* 68:064204

Fortney J, Hubbard WB. 2003. Phase separation in giant planets: inhomogeneous evolution of Saturn. *Icarus* 164:228–43

Gautier D, Hersant F, Mousis O, Lunine JI. 2001. Enrichments in volatiles in Jupiter: A new interpretation of the Galileo measurements. *Ap. J. Lett.* 550:L227–30

Gautier D, Owen T. 1989. The composition of outer planet atmospheres. In *Origin and Evolution of Planetary and Satellite Atmospheres*, ed. SK Atreya, JB Pollack, MS Matthews, pp. 487–512. Tucson: Univ. Ariz. Press

Goukenleuque C, Bézard B, Joguet B, Lellouch E, Freedman R. 2000. A radiative equilibrium model of 51 Peg b. *Icarus* 143:308

Gregoryanz E, Goncharov AF, Matsuishi K, Mao H, Hemley RJ. 2003. Raman spectroscopy of hot dense hydrogen. *Phys. Rev. Lett.* 90:175701-1–4

Gu P-G, Bodenheimer PH, Lin DNC. 2004. The internal structural adjustment due to tidal heating of short-period inflated giant planets. *Ap. J.* 608:1076–94

Guillot T. 1995. Condensation of methane ammonia and water in the inhibition of convection in giant planets. *Science* 269:1697–99

Guillot T. 1999a. A comparison of the interiors of Jupiter and Saturn. *Planet. Space. Sci.* 47:1183–200

Guillot T. 1999b. Interior of giant planets inside and outside the Solar System. *Science* 286:72–77

Guillot T, Chabrier G, Gautier D, Morel P. 1992. Effect of radiative transport on the

evolution of Jupiter and Saturn. *Ap. J.* 450: 463–72

Guillot T, Gautier D, Chabrier G, Mosser B. 1994. Are the giant planets fully convective? *Icarus* 112:337–53

Guillot T, Burrows A, Hubbard WB, Lunine JI, Saumon D. 1996. Giant planets at small orbital distances. *Ap. J.* 459:L35–38

Guillot T, Gladman B. 2000. Late planetesimal delivery and the composition of giant planets. In *Proceedings of the Disks, Planetesimals and Planets Conference, ASP Conference Series*, ed. Astron. Soc. Pacific, 219:475–85

Guillot T, Showman A. 2002. Evolution of "51 Pegasus b-like" planets. *Astron. Astrophys.* 385:156–65

Guillot T, Stevenson DJ, Hubbard WB, Saumon D. 2004. The interior of Jupiter. In *Jupiter: The Planet, Satellites, and Magnetosphere*, ed. F Bagenal, W McKinnon, T Dowling. Cambridge, UK: Cambridge Univ. Press

Henry GW, Marcy GW, Butler RP, Vogt SS. 2000. A transiting "51 Peg-like" planet. *Ap. J.* 529:L41–44

Hersant F, Gautier D, Lunine JI. 2004. Enrichment in volatiles in the giant planets of the Solar System. *Planet. Space Sci.* 52:623–41

Holmes NC, Ross M, Nellis WJ. 1995. Temperature measurements and dissociation of shock-compressed liquid deuterium and hydrogen. *Phys. Rev. B* 52:15835–45

Hubbard WB. 1968. Thermal structure of Jupiter. *Ap. J.* 152:745–54

Hubbard WB. 1977. The Jovian surface condition and cooling rate. *Icarus* 30:305–10

Hubbard WB. 1982. Effects of differential rotation on the gravitational figures of Jupiter and Saturn. *Icarus* 52:509–15

Hubbard WB. 1999. Gravitational signature of Jupiter's deep zonal flows. *Icarus* 137:196–99

Hubbard WB, Burrows A, Lunine JI. 2002. Theory of Giant Planets. *Annu. Rev. Astron. Astrophys.* 40:103–36

Hubbard WB, Guillot T, Marley MS, Burrows A, Lunine JI, Saumon DS. 1999. Comparative evolution of Jupiter and Saturn. *Planet. Space. Sci.* 47:1175–82

Hubbard WB, Pearl JC, Podolak M, Stevenson DJ. 1995. The interior of Neptune. In *Neptune and Triton*, ed. DP Cruikshank, pp. 109–38. Tucson: Univ. Ariz. Press

Iro N, Bézard B, Guillot T. 2004. A time-dependent radiative model of HD209458b. *Icarus.* In press

Knudson MD, Hanson DL, Bailey JE, Hall CA, Asay JR, Anderson WW. 2002. Equation of state measurements in liquid deuterium to 70 GPa. *Phys. Rev. Lett.* 87:225501

Knudson MD, Hanson DL, Bailey JE, Hall CA, Asay JR, Deeney C. 2004. Principal Hugoniot, reverberating wave, and mechanical reshock measurements of liquid deuterium to 400 GPa using plate impact techniques. *Phys. Rev. B* 69:144209

Konacki M, Torres G, Jha S, Sasselov DD. 2003. An extrasolar planet that transits the disk of its parent star. *Nature* 421:507–9

Konacki M, Torres G, Sasselov DD, Pietrzynski G, Udalski A, et al. 2004. The transiting extrasolar giant planet around the star OGLE-TR-113. *Ap. J.* 609:L37–40

Lammer H, Selsis F, Ribas I, Guinan EF, Bauer SJ, Weiss WW. 2003. Atmospheric loss of exoplanets resulting from stellar X-ray and extreme-ultraviolet heating. *Ap. J.* 598:L121–4

Laughlin G, Wolf A, Vanmunster T, Bodenheimer P, Fischer D, et al. 2004. A comparison of observationally determined radii with theoretical radius predictions for short-period transiting extrasolar planets. *Ap. J.* In press

Lecavelier des Etangs A, Vidal-Madjar A, McConnell JC, Hébrard G. 2004. Atmospheric escape from hot Jupiters. *Astron. Astrophys.* 418:L1–4

Lenzuni P, Chernoff DF, Salpeter EE. 1991. Rosseland and Planck mean opacities of a zero-metallicity gas. *Ap. J. Suppl.* 76:759–801

Levison HF, Morbidelli A. 2003. The formation of the Kuiper belt by the outward transport of bodies during Neptune's migration. *Nature* 426:419–21

Lin DNC, Bodenheimer P, Richardson DC. 1996. Orbital migration of the planetary companion of 51 Pegasi to its present location. *Nature* 380:606–7

Lindal GF. 1992. The atmosphere of Neptune—an analysis of radio occultation data acquired with Voyager 2. *Astron. J.* 103:967–82

Lindal GF, Sweetnam DN, Eshleman VR. 1985. The atmosphere of Saturn—an analysis of the Voyager radio occultation measurements. *Astron. J.* 90:1136–46

Lindal GF, Wood GE, Levy GS, Anderson JD, Sweetnam DN, et al. 1981. The atmosphere of Jupiter—an analysis of the Voyager radio occultation measurements. *J. Geophys. Res.* 86:8721–27

Lodders K. 2003. Solar System abundances and condensation temperatures of the elements. *Ap. J.* 591:1220–47

Lubow SH, Tout CA, Livio M. 1997. Resonant tides in close orbiting planets. *Ap. J.* 484:866–70

Magalhães JA, Seiff A, Young RE. 2002. The stratification of Jupiter's troposphere at the Galileo probe entry site. *Icarus* 158:410–33

Mahaffy PR, Niemann HB, Alpert A, Atreya SK, Demick J, et al. 2000. Noble gas abundance and isotope ratios in the atmosphere of Jupiter from the Galileo Probe Mass Spectrometer. *J. Geophys. Res.* 105:15061–72

Mao H, Hemley RJ. 1994. Ultrahigh-pressure transitions in solid hydrogen. *Rev. Mod. Phys.* 66:671–92

Marcy GW, Butler RP, Williams E, Bildsten L, et al. 1997. The planet around 51 Pegasi. *Ap. J.* 481:926–35

Marley MS, Gomez P, Podolak P. 1995. Monte Carlo interior models for Uranus and Neptune. *J. Geophys. Res.* 100:23349–54

Marley MS, McKay CP. 1999. Thermal structure of Uranus' atmosphere. *Icarus* 138:268–86

Militzer B, Ceperley DM. 2001. Path integral Monte Carlo simulation of the low-density hydrogen plasma. *Phys. Rev. E* 63:6404

Moutou C, Pont F, Bouchy F, Mayor M. 2004. Accurate radius and mass of the transiting exoplanet OGLE-TR-132b. *Astron. Astrophys.* 424:L31

Niemann HB, Atreya SK, Carignan GR, Donahue TM, Haberman JA, et al. 1998. The composition of the Jovian atmosphere as determined by the Galileo probe mass spectrometer. *J. Geophys. Res.* 103:22831–38

Ogilvie GI, Lin DNC. 2004. Tidal dissipation in rotating giant planets. *Ap. J.* 610:477–509

Owen T, Mahaffy P, Niemann HB, Atreya S, Donahue T, et al. 1999. A low-temperature origin for the planetesimals that formed Jupiter. *Nature* 402:269–70

Pätzold M, Rauer H. 2002. Where are the massive close-in extrasolar planets? *Ap. J.* 568:L117–20

Pearl JC, Conrath BJ. 1991. The albedo, effective temperature, and energy balance of Neptune, as determined from Voyager data. *J. Geophys. Res. Suppl.* 96:18921–29

Pfaffenzeller O, Hohl D, Ballone P. 1995. Miscibility of hydrogen and helium under astrophysical conditions. *Phys. Rev. Lett.* 74:2599–602

Podolak M, Hubbard WB, Stevenson DJ. 1991. Model of Uranus' interior and magnetic field. In *Uranus*, ed. JT Bergstralh, ED Miner, MS Matthews, pp. 29–61. Tucson: Univ. Ariz. Press

Podolak M, Podolak JI, Marley MS. 2000. Further investigations of random models of Uranus and Neptune. *Planet. Space Sci.* 48: 143–51

Podolak M, Weizman A, Marley MS. 1995. Comparative models of Uranus and Neptune. *Planet. Space Sci.* 43:1517–22

Pollack JB, Hubickyj O, Bodenheimer P, Lissauer JJ, Podolak M, Greenzweig Y. 1996. Formation of the giant planets by concurrent accretion of solids and gas. *Icarus* 124:62

Pont F, Bouchy F, Queloz D, Santos NC, Melo C, et al. 2004. The "missing link": A 4-day period transiting exoplanet around OGLE-TR-111. *Astron. Astrophys.* 426:L15

Rasio F, Tout CA, Lubow SH, Livio M. 1996. Tidal decay of close planetary orbits. *Ap. J.* 470:1187–91

Ross M. 1998. Linear-mixing model for shock-compressed liquid deuterium. *Phys. Rev. B* 58:669

Ross M, Yang LH. 2001. Effect of chainlike structures on shock-compressed liquid deuterium. *Phys. Rev. B* 64:134210

Roos-Serote M, Atreya SK, Wong MK, Drossart P. 2004. On the water abundance in the atmosphere of Jupiter. *Planet. Space Sci.* 52:397–414

Roulston, MS, Stevenson DJ. 1995. Prediction of neon depletion in Jupiter's atmosphere. *EOS* 76:343 (Abstr.)

Sasselov DD. 2003. The new transiting planet OGLE-TR-56b: orbit and atmosphere. *Ap. J.* 596:1327–31

Saumon D, Chabrier G, Van Horn HM. 1995. An equation of state for low-mass stars and giant planets. *Ap. J. Suppl.* 99:713–41

Saumon D, Chabrier G, Wagner DJ, Xie X. 2000. Modeling pressure-ionization of hydrogen in the context of astrophysics. *High Press. Res.* 16:331–43

Saumon D, Guillot T. 2004. Shock compression of deuterium and the interiors of Jupiter and Saturn. *Ap. J.* 609:1170–80

Saumon D, Hubbard WB, Burrows A, Guillot T, Lunine JI, Chabrier G. 1996. A theory of extrasolar giant planets. *Ap. J.* 460:993–1018

Saumon D, Hubbard WB, Chabrrier G, Van Horn HM. 1992. The role of the molecular-metallic transition of hydrogen in the evolution of Jupiter, Saturn and brown dwarfs. *Ap. J.* 391:827–31

Seager S, Sasselov DD. 1998. Extrasolar giant planets under strong stellar irradiation. *Ap. J.* 502:L157–60

Seager S, Sasselov DD. 2000. Theoretical transmission spectra during extrasolar giant planet transits. *Ap. J.* 537:916–21

Seager S, Hui L. 2002. Constraining the rotation rate of transiting extrasolar planets by oblateness measurements. *Ap. J.* 574:1004–10

Seiff A, Kirk DB, Knight TCD, Young RE, Mihalov JD, et al. 1998. Thermal structure of Jupiter's atmosphere near the edge of a 5-μm hot spot in the north equatorial belt. *J. Geophys. Res.* 103:22857–90

Showman AP, Guillot T. 2002. Atmospheric circulation and tides of "51 Pegasus b-like" planets. *Astron. Astrophys.* 385:166–80

Sozzetti A, Young D, Torres G, Charbonneau D, Latham DW, et al.. 2004, High-resolution spectroscopy of the transiting planet host Star TrES-1. *Ap. J. Lett.* 616:L167–70 (astro-ph/04106693)

Stevenson DJ, Salpeter EE. 1977. The dynamics and helium distribution in hydrogen-helium fluid planets. *Ap. J. Suppl.* 35:239–61

Stevenson DJ. 1982. Interiors of the giant planets. *Annu. Rev. Earth Planet. Sci.* 10:257–95

Stevenson DJ. 1985. Cosmochemistry and structure of the giant planets and their satellites. *Icarus* 62:4–15

Sudarsky D, Burrows A, Hubeny I. 2003. Theoretical spectra and atmospheres of extrasolar giant planets. *Ap. J.* 588:1121–48

Torres G, Konacki M, Sasselov DD, Jha S. 2004. New data and improved parameters for the extrasolar transiting planet OGLE-TR-56b. *Ap. J.* 609:1071–75

Trilling DE, Benz W, Guillot T, Lunine JI, Hubbard WB, Burrows A. 1998. Orbital evolution and migration of giant planets: Modeling extrasolar planets. *Ap. J.* 500:428–39

Trilling DE, Lunine JI, Benz W. 2002. Orbital migration and the frequency of giant planet formation. *Astron. Astrophys.* 394:241–51

Tyler GL, Sweetnam DN, Anderson JD, Borutzki SE, Campbell JK, et al. 1989. Voyager radio science observations of Neptune and Triton. *Science* 246:1466–73

Vidal-Madjar A, Désert J-M, Lecavelier des Etangs A, Hébrard G, Ballester GE, et al. 2004. Detection of oxygen and carbon in the hydrodynamically escaping atmosphere of the extrasolar planet HD 209458b. *Ap. J.* 604:L69–72

Vidal-Madjar A, Lecavelier des Etangs A, Désert J-M, Ballester GE, Ferlet R, et al. 2003. An extended upper atmosphere around the extrasolar planet HD209458b. *Nature* 422:143–46

von Zahn U, Hunten DM, Lehmacher G. 1998. Helium in Jupiter's atmosphere: results from the Galileo probe helium interferometer experiment. *J. Geophys. Res.* 103:22815–30

Warwick JW, Evans DR, Peltzer GR, Peltzer RG, Roming JH, et al. 1989. Voyager planetary radio astronomy at Neptune. *Science* 246:1498–501

Warwick JW, Evans DR, Roming JH, Sawyer CB, Desch MD, et al. 1986. Voyager 2 radio observations of Uranus. *Science* 233:102–6

Weir ST, Mitchell AC, Nellis WJ. 1996. Metallization of fluid molecular hydrogen at 140 GPa (1.4 Mbar). *Phys. Rev. Lett.* 76:1860–63

Witte MG, Savonije GJ. 2002. Orbital evolution by dynamical tides in solar type stars. Application to binary stars and planetary orbits. *Astron. Astrophys.* 386:222–36

Zharkov VN, Trubitsyn VP. 1974. Determination of the equation of state of the molecular envelopes of Jupiter and Saturn from their gravitational moments. *Icarus* 21:152–56

Zharkov VN, Trubitsyn VP. 1978. *Physics of Planetary Interiors*, ed. WB Hubbard. Tucson, AZ: Pachart

Annual Review of Earth and Planetary Sciences
Volume 33, 2005

CONTENTS